NBSIR 74-457

Transmission of Electrons Through Foils

Stephen Michael Seltzer

Center for Radiation Research
Institute for Basic Standards
National Bureau of Standards
Washington, D. C. 20234

April 1974

Prepared for
Office of Naval Research
Arlington, Virginia 22217

NBSIR 74-457

TRANSMISSION OF ELECTRONS THROUGH FOILS

Stephen Michael Seltzer

Center for Radiation Research
Institute for Basic Standards
National Bureau of Standards
Washington, D. C. 20234

April 1974

Prepared for
Office of Naval Research
Arlington, Virginia 22217

U. S. DEPARTMENT OF COMMERCE, Frederick B. Dent, Secretary

NATIONAL BUREAU OF STANDARDS, Richard W. Roberts, Director

TRANSMISSION OF ELECTRONS THROUGH FOILS*

by

Stephen Michael Seltzer

The transmission of electrons through foils has been studied by a Monte Carlo method. Cases involving electrons with energies from 50 keV to 1 MeV normally incident on beryllium, mylar, aluminum, and titanium foils are considered. Good agreement with experimental results has been found for quantities such as the number transmission, the energy and angular distribution of the emergent electrons, and the spatial distribution of energy deposited in the foil.

A comprehensive set of results has been generated for 100, 150, 200, 300 and 400-keV electrons incident on beryllium, mylar, aluminum and titanium foils that are commonly used as vacuum windows in conjunction with low energy electron accelerators. Quantities given are the electron number and energy transmission and reflection, the energy absorbed, and the energy and angular distribution of the transmitted electrons. It is shown that much of the results can be presented in a scaled form which reduces the explicit dependence on, and facilitates the interpolation with respect to, the incident energy.

*/ This report is based on a Thesis submitted to the Faculty of the Graduate School of the University of Maryland in partial fulfillment of the requirements for the degree of Master of Science 1973.

ACKNOWLEDGMENTS

I wish to thank Dr. Raymond Hayward, my thesis advisor, for his many useful comments on this work. I would also like to express my gratitude to Dr. Martin Berger who provided guidance and suggestions over the course of this work.

Dr. Robert Placious suggested the problem treated in this work, and conversations with him and Dr. William McLaughlin directed my attention to the applications of the results presented here.

Finally, I wish to thank my mother, Mrs. Henrietta Seltzer, for the time and effort she contributed in the preparation of this manuscript.

TABLE OF CONTENTS

CHAPTER		PAGE
I.	INTRODUCTION	1
II.	BACKGROUND	3
	A. Energy Loss	3
	1. Single Inelastic Scattering	3
	2. Stopping Power	4
	3. Multiple-Scattering Distribution of Energy Losses	7
	B. Angular Deflections	10
	1. Single Elastic Scattering	10
	2. Multiple-Scattering Distribution of Angular Deflections	11
	C. Coupling of One-Variable Multiple Scattering Theories	13
	D. Solutions of the Multi-Variable Transport Equation	15
III.	METHOD OF CALCULATION	17
	A. Theoretical Distributions	17
	B. Transport Model	19
	1. Definition of Boundary Conditions and Quantities Calculated	19
	2. Division of Electron Tracks into Segments	21
	3. Generation of Electron Histories	22
IV.	COMPARISON WITH EXPERIMENT	26
V.	NEW RESULTS	32
VI.	COMPARISON WITH SIMPLE THEORY	35

CHAPTER PAGE

FIGURES..... 37

TABLES..... 54

APPENDIX. TABLES OF TRANSMITTED ELECTRON CURRENT..... 69

REFERENCES..... 128

LIST OF FIGURES

FIGURE		PAGE
1.	Comparison of experimental and calculated number transmission coefficients T_N for aluminum. The foil thickness z is expressed in terms of the ratio z/r_o, where r_o is the mean range of an electron incident with energy E_o. The solid curves are calculated values of T_N and pertain to the transmitted charge. The dashed curves are calculated such that the emergence of a primary electron and one or more associated secondary electrons is treated as a single "transmission event" (corresponding to the experimental conditions of Seliger).....	37
2.	Comparison of experimental and calculated number transmission coefficients T_N for beryllium. The foil thickness z is expressed in terms of the ratio z/r_o, where r_o is the mean range of an electron incident with energy E_o.....	38
3.	Comparison of experimental and calculated number transmission coefficients T_N for 1-MeV electrons incident on titanium foils. The foil thickness z is expressed in terms of the ratio z/r_o, where r_o is the mean range of the incident electrons.....	39
4.	Comparison of experimental and calculated angular distributions of electrons transmitted through aluminum foils of thickness z. The incident energy E_o is 1 MeV; the angular distributions shown include all electrons transmitted with energies greater than 100 keV.....	40
5.	Comparison of experimental and calculated energy spectra of electrons transmitted through aluminum foils of thickness z. The incident energy E_o is 1 MeV; the energy spectra shown include all electrons transmitted, regardless of angle.....	41
6.	Comparison of experimental and calculated energy spectra of electrons reflected from an aluminum foil. The incident energy E_o is 0.5 MeV; the energy spectra shown include all electrons reflected regardless of angle...	42

FIGURE PAGE

7. Comparison of experimental and calculated distributions of energy deposition as a function of depth. The quantity shown is the scaled energy deposition distribution $\frac{r_o D(z)}{E_o}$, where E_o is the energy and r_o the mean range of the incident electrons. The results for Be, Al, and Cu for E_o=0.5 MeV are for a broad beam of electrons incident perpendicularly on a semi-infinite medium. The results for Al for E_o= 0.1 MeV are for a plane perpendicular source in an unbounded medium, i.e., with backing material behind the source plane. The experimental distributions have been normalized so as to give the same total energy deposited as the calculations..... 43

8. Universal curves of number transmission and energy absorption coefficients for titanium foils. The curves are composites drawn through the Monte Carlo results (shown as points) for the number transmission coefficient T_N and the energy absorption coefficient Φ_A. The foil thickness z is expressed as a fraction of the mean range r_o of the incident electrons..... 44

9. Universal curves of the most probable energy and the full-width at half-maximum of the spectra of electrons transmitted through titanium foils. The curves are composites drawn through the Monte Carlo results (shown as points) for the most probable energy E_p and the full-width at half-maximum W as fractions of the incident energy E_o. The foil thickness z is expressed as a fraction of the mean range r_o of the incident electrons..... 45

10. Normalized energy spectra of transmitted electrons. The quantity shown is $E_o S(E,z)/T_N$, where E_o is the incident energy, $S(E,z)$ the energy spectrum and T_N the number transmission coefficient.

    a. Dependence on foil thickness; titanium, E_o=200 keV.

    b. Dependence on incident energy; titanium, z = 1 mil (11.43 mg/cm^2).

    c. Dependence on foil material; E_o=200 keV, z=2 mils 46

FIGURE PAGE

11. Percentile cosines for electrons transmitted through beryllium, mylar, aluminum, and titanium foils. A percentage P of the electrons transmitted by a foil of given thickness emerge with direction cosines between $\cos\theta_P$ and 1.0. Foil thickness z is expressed as a fraction of the mean range r_o of the incident electrons. The curves are composites drawn through the Monte Carlo results shown as points:

☆ E_o=100 keV
△ 150
□ 200
▽ 300
○ 400 47

12. Equilibrium shapes of the cumulative angular distributions of electrons transmitted through thick foils. The curves give the fraction of the transmitted electrons that have direction cosines between $\cos\theta$ and 1.0..... 48

13. Normalized angular distributions of transmitted electrons. The quantity shown is the angular distribution $A(\theta,z)$ divided by the number transmission coefficient T_N.

a. Dependence on foil thickness; titanium, E_o=200 keV.

b. Dependence on incident energy; titanium, z=1 mil (11.43 mg/cm^2).

c. Dependence on foil material; E_o=200 keV, z=2 mils. 49

14. Current, differential in energy and angle, of electrons transmitted through a 1-mil(11.43 mg/cm^2) titanium foil. The incident energy E_o is 200 keV. The histograms represent calculated values of the transmitted current, $J(E,\theta,z)$. The curves give the quantity $S(E,z)A(\theta,z)/T_N$, where $S(E,z)$ is the calculated energy spectrum (regardless of angle), $A(\theta,z)$ the calculated angular distribution (regardless of energy) and T_N the number transmission coefficient.

a. Averaged over the interval $0^o \leq \theta \leq 10^o$.

b. Averaged over the interval $30^o \leq \theta \leq 40^o$.

c. Averaged over the interval $60^o \leq \theta \leq 70^o$..... 50

FIGURE PAGE

15. Most probable energy of electrons transmitted through planar silicon detectors. The quantity shown is the most probable E_p as a fraction of the incident energy E_o. The detector thickness z is expressed as a fraction of the mean range r_o of the incident electrons. The solid curve is a composite drawn through the Monte Carlo results (shown as points). The dashed curves are from Landau's energy loss theory, without inclusion of multiple scattering detours..... 51

16. Comparison of Monte Carlo results and Landau-Blunck-Leisegang theory. Given are the most probable energy E_p and the full-width at half-maximum W of the spectrum of electrons transmitted through titanium foils of thickness z. Curves obtained from the Monte Carlo results are labeled MC; from Landau's theory, L; and from the theory of Blunck and Leisegang, LBL..... 52

17. Mean deflection cosine as given by the complete Monte Carlo calculation and as derived from the theory of Goudsmit and Saunderson. The dashed curves, from the Goudsmit-Saunderson theory (labeled A), pertain to the flux of electrons having traveled pathlength z in an unbounded medium. Plotted versus z/r_o, where r_o is the mean range of the incident electrons, the dashed curves represent results for 100 keV $\leq E_o \leq$ 400 keV. The Monte Carlo results pertain to the current of electrons transmitted by a foil of thickness z and are represented by the solid curves (labeled MC) drawn through the points:

☆ E_o=100 keV
△ 150
□ 200
▽ 300
○ 400 53

LIST OF TABLES

TABLE		PAGE
1.	Properties of foils considered in this paper.....	54
2.	Electron stopping power and range. Powers of ten are shown in parentheses; e.g., 5.21(-3) means 5.21×10^{-3}.....	55
3.	Dependence of calculated electron transmission on the step-size parameter n used in the Monte Carlo model. The average fractional energy loss per step was 0.083/n. Results are for 200-keV electrons incident on a 2-mil (13.72 mg/cm^2) aluminum foil, and are based on a sample of 20,000 Monte Carlo histories. Quantities given are: T_N, number transmission coefficient; R_N, number reflection coefficient; T_E, energy transmission coefficient; Φ_A, energy absorption coefficient; R_E, energy reflection coefficient; E_{av}/E_o, mean energy of transmitted electrons as fraction of incident energy; $\langle \cos\theta \rangle_{av}$, mean deflection cosine of transmitted electrons.....	56
4.	Transmission, reflection and absorption of electron beams incident on beryllium, mylar, aluminum and titanium foils. Quantities given are: T_N, number transmission coefficient; R_N, number reflection coefficient; T_E, energy transmission coefficient; Φ_A, energy absorption coefficient; R_E, energy reflection coefficient.....	57
5.	Characteristics of the energy spectra of electrons transmitted through beryllium, mylar, aluminum and titanium foils. Quantities given are: E_{av}/E_o, mean energy as fraction of incident energy, E_p/E_o, most probable energy as fraction of incident energy; W/E_o, full-width at half-maximum as fraction of incident energy; W/E_p, full-width at half-maximum as fraction of most probable energy.....	61
6.	Cumulative angular distribution of electrons transmitted through beryllium, mylar, aluminum and titanium foils. The quantity given is the fraction of the transmitted electrons that emerge in directions between 0^o and θ.....	65

I. INTRODUCTION

An electron traveling through a foil undergoes a succession of inelastic and elastic collisions, causing changes in its energy and direction. Thus, a beam of electrons, originally monoenergetic and monodirectional, can have broad energy and angular distributions after passing through a foil; if the foil is of sufficient thickness, a significant fraction of the incident electrons will be completely absorbed. The purpose of this work is to report on Monte Carlo calculations of these effects for electrons incident with energies from 1 MeV down to about 100 keV. Our goal is two-fold: first, to verify the Monte Carlo model through comparisons with appropriate experiments, and second, to generate a comprehensive set of transmission data for beryllium, mylar, aluminum, and titanium foils for incident electron energies from 100 to 400 keV.

Such foils are frequently used as windows for bringing out of the vacuum region a beam of electrons generated by an accelerator. These windows may be present for a variety of reasons: a) They are used in many experimental configurations in order to avoid the problems associated with oil contamination of a target in the vacuum system or with the changing of targets. b) In order to obtain broad beam irradiation geometries, a foil may be purposely introduced to "spread" the beam by broadening its angular distribution. c) A gaseous target must be enclosed, with a window present to allow entrance to the electrons. An interesting example of this is in the recently developed electron-beam-controlled gas-discharge laser.[1,2] d) Electron accelerators are finding growing use in industrial radiation processing.[3]

In these situations, in which large samples are moved through an electron beam, practicality dictates the use of a window.

A foil a few mils* thick is nearly transparent to high energy electron beams. In such cases, the effects of scattering are small and can be calculated using available analytical theories. However, for electron energies below about 0.5 MeV, the angular deflection and energy loss begin to be appreciable. For this reason, incident energies between 100 keV and 400 keV were emphasized in the present calculations. So that the results would be more directly applicable to situations of interest, the calculations were made for foils of readily available thickness: 2, 3 and 5-mil beryllium; 1/4, 1/2 and 1-mil mylar; and 1/2, 1 and 2 mils for both aluminum and titanium. The quantities obtained include the fraction of the incident current and energy that is transmitted, the amount of energy absorbed by the foil, and the energy and angular distributions of the transmitted electrons. These results will aid in the selection of an optimum window by a balance of mechanical and thermal requirements, on the one hand, and desired transmitted current and spectral and angular properties of the transmitted beam, on the other. In addition, for a given window, knowledge of the characteristics of the transmitted beam is important in the design and analysis of experiments employing these beams.

---

*The mil is commonly used as a unit of thickness for commercially available foils in the United States. One mil = 1/1000th of an inch = 25.4 μm.

II. BACKGROUND

The basic interactions that govern the passage of electrons through matter have been reviewed by several authors including Evans,[4] Rossi,[5] Bethe and Askin,[6] Fano,[7] Birkhoff,[8] Berger,[9] and Zerby and Keller.[10] In these articles, various theories of single and multiple Coulomb scattering are summarized and compared with the results of numerous measurements. Here we will consider the pertinent single-scattering cross sections and discuss multiple scattering theories with an eye toward developing an accurate description of the electron penetration process.

A. Energy Loss

1. Single Inelastic Scattering

Simple classical considerations lead to a cross section for the scattering of electrons by free electrons

$$\frac{d\sigma}{d\epsilon} = \frac{2\pi e^4}{mv^2E}\,\frac{1}{\epsilon^2} \quad , \tag{1}$$

where ϵ is the fractional energy transfer in units of the incident kinetic energy E.

Møller,[11] using a relativistic theory which includes spin and exchange effects, derived the cross section

$$\frac{d\sigma}{d\epsilon} = \frac{2\pi e^4}{mv^2E}\left\{\frac{1}{\epsilon^2} + \frac{1}{(1-\epsilon)^2} + \left(\frac{\tau}{\tau+1}\right)^2 - \frac{2\tau+1}{(\tau+1)^2}\,\frac{1}{\epsilon(1-\epsilon)}\right\} \quad , \tag{2}$$

where $\tau = E/mc^2$. With the energy transfer ϵ is associated the angular deflection ω_p (in the laboratory system) of the primary electron

$$\cos^2\omega_p = \frac{(1-\epsilon)(\tau+2)}{(1-\epsilon)\tau+2} \quad . \tag{3}$$

The angular deflection ω_s of the secondary electron is obtained from

$$\cos^2\omega_s = \frac{\epsilon(\tau+2)}{\epsilon\tau+2} \quad . \tag{4}$$

The probability per unit pathlength of an inelastic scattering with fractional energy transfer greater than a given cut-off value, $\epsilon > \epsilon_c$, can be obtained from the Møller formula:

$$\frac{N_a Z}{A}\int_{\epsilon_c}^{1/2}\frac{d\sigma}{d\epsilon}\,d\epsilon = \frac{N_a Z}{A}\frac{2\pi e^4}{mv^2E}\left\{\frac{1}{\epsilon_c}-\frac{1}{1-\epsilon_c}+\left(\frac{\tau}{\tau+1}\right)^2\left(\frac{1}{2}-\epsilon_c\right) - \frac{2\tau+1}{(\tau+1)^2}\ln\left(\frac{1-\epsilon_c}{\epsilon_c}\right)\right\} \quad , \tag{5}$$

where N_a is Avagadro's number, Z the atomic number of the medium, and A the atomic weight. The integral in Eq.(5) extends only to $\epsilon = 1/2$ because the outgoing electron of higher energy is, by definition, the primary electron.

2. Stopping Power

The mean collision energy loss per unit pathlength - the collision loss stopping power - is defined as

$$L_c(E) = \frac{N_a Z}{A}\int_0^{1/2}\epsilon\frac{d\sigma}{d\epsilon}\,d\epsilon \quad . \tag{6}$$

Eq.(6) is evaluated by separating the integral into the two intervals $0 \le \epsilon \le \epsilon'$ and $\epsilon' \le \epsilon \le 1/2$, where ϵ' E is a small energy but one that is large compared to that of the atomic electrons. In the first interval, the binding of the atomic electrons is taken into account through Bethe[12] stopping power theory:

$$\frac{N_a Z}{A}\int_0^{\epsilon'}\epsilon\frac{d\sigma}{d\epsilon}\,d\epsilon = \frac{N_a Z}{A}\frac{2\pi e^4}{mv^2}\left\{\ln\left[\frac{2mc^2\epsilon' E\beta^2}{(1-\beta^2)\,I^2}\right]-\beta^2\right\} \quad , \tag{7}$$

where I is the mean excitation energy for the medium.

In the second interval, $\epsilon \geq \epsilon'$, the binding of the atomic electrons is assumed negligible, and the Møller cross section is applicable. When the integral over the Møller cross section is combined with Eq.(7), the parameter ϵ' drops out, and the final result is

$$L_c(E) = \frac{N_a Z}{A} \frac{2\pi e^4}{m v^2} \left\{ \ln\left[\frac{E^2(\tau+2)}{2I^2}\right] + 1 - \beta^2 + \left[\frac{\tau^2}{8} - (2\tau+1)\ln 2\right]/(\tau+1)^2 - \delta \right\} . \tag{8}$$

The quantity δ in Eq.(8) is the density effect correction factor which gives the reduction in the collision loss due to the dielectric polarization of the medium. Sternheimer and Peierls[13] give a general expression for δ, based on a fit to calculated values:

$$\delta = \begin{cases} 0 & , X \leq X_0 \\ 4.606X + C + a(X_1 - X)^d & , X_0 < X < X_1 \\ 4.606X + C & , X \geq X_1 \end{cases} , \tag{9}$$

where

$$X = \log_{10}(p/mc) , \tag{10}$$

and

$$C = -2\ln(I/h\nu_p) - 1 . \tag{11}$$

In Eq.(11), $h\nu_p$ is the plasma energy for the medium,

$$h\nu_p = \left[\frac{\rho N_a Z}{A} \frac{e^2 h^2}{\pi m}\right]^{1/2} = 28.8\left(\rho Z/A\right)^{1/2} \text{eV} , \tag{12}$$

where ρ is the density of the medium (in g/cm^3 for the second equality in Eq.(12)). The parameter a is obtained from the expression

$$a = \frac{-C - 4.606 X_0}{(X_1 - X_0)^d} \quad , \tag{13}$$

and X_0 and X_1 for solids and liquids* are determined as follows:

For $I < 100$ eV, $d = 3$, $X_1 = 2$ and

$$X_0 = \begin{cases} 0.2 & , -C < 3.681 \\ -0.326\,C - 1.0 & , -C \geq 3.681 \end{cases} \tag{14a}$$

For $I \geq 100$ eV, $d = 3$, $X_1 = 3$ and

$$X_0 = \begin{cases} 0.2 & , -C < 5.215 \\ -0.326\,C - 1.5 & , -C \geq 5.215 \end{cases} \tag{14b}$$

The mean energy loss by bremsstrahlung was evaluated using a package of bremsstrahlung production cross sections discussed in detail by Berger and Seltzer.[14] This package consists of Born-approximation formulas combined with screening, Coulomb, and high-frequency correction factors. Although it is included, the bremsstrahlung energy loss is of minor importance in the present calculations; in the cases considered here, less than about 2% of the initial kinetic energy of the electron is converted into bremsstrahlung photons.

---

*The parameters for gases and liquid hydrogen are given in Reference 13.

The total stopping power L(E), the sum of the collision and bremsstrahlung mean energy losses per unit pathlength, is used to define the mean range r_o:

$$r_o(E) = \int_0^E \frac{dE'}{L(E')} \quad . \tag{15}$$

Defined as above, the mean range is the total pathlength* travelled by an electron in the continuous-slowing-down approximation. The collision energy loss formula ceases to be valid at energies comparable to the binding energies of the atomic electrons; so the zero lower limit of the integral in Eq.(15) was replaced by a cut-off energy of about 1 keV, and a small estimated residual range was added to the result. For initial energies E greater than about 10 keV, this residual range is negligible. The calculations of stopping power and range are similar to those in previous tabulations.[15,16] Parameters entering into the energy loss formula are given in Table 1, and stopping powers and ranges are given in Table 2 for beryllium, mylar, aluminum, and titanium.

3. Multiple-Scattering Distribution of Energy Losses

Williams[17] and Landau[18] developed multiple scattering theories which give the distribution of the energy losses Δ resulting from successive inelastic collisions along a given pathlength s - the so-called energy-loss straggling distribution. In both theories,

---

*Note that the mean range refers to pathlength and not to depth of penetration, which is largely determined by multiple elastic scattering detours.

the single scattering cross section of Eq.(1) was used,

$$\frac{d\sigma}{dk} = \frac{2\pi e^4}{mc^2\beta^2}\,\frac{1}{k^2} \quad , \tag{1'}$$

where k is the energy transfer (not fractional energy transfer). The cross section is assumed independent of Δ along s ($\beta^2 = \beta_o^2$) implying the restriction $\Delta \ll E$. The use of this cross section does not take into account the binding of the atomic electrons, implying the further restriction $\Delta \gg \epsilon' E$. Both authors arrive at similar distributions, but Landau's results - presented in a more convenient form - have wider use.

Landau allowed possible energy transfers in a single collision to extend to infinity. His result is a distribution that can be expressed in terms of a universal function of a single scaled energy variable,

$$f(\Delta,s)\,d\Delta = \varphi(\lambda)\,d\lambda \quad , \tag{16}$$

where

$$\lambda = \frac{\Delta}{\xi} - \ln\left[\frac{2\xi mc^2\beta^2}{(1-\beta^2)\,I^2}\right] + \beta^2 - 0.423 \quad , \tag{17}$$

and

$$\xi = \frac{N_a Z}{A}\,\frac{2\pi e^4}{mc^2\beta^2}\,s. \tag{18}$$

The universal function of $\varphi(\lambda)$ is given by

$$\varphi(\lambda) = \frac{1}{2\pi i}\int_{-i\infty+c}^{+i\infty+c} \exp(u\ln u + \lambda u)\,du \quad , \tag{19}$$

and has been accurately evaluated and tabulated by Börsch-Supan.[19] According to his tabulation, $\varphi(\lambda)$ has a maximum at $\lambda = -0.225$ and a

full-width at half-maximum of $4.02\,\xi$. The same values of the most probable λ and width of the distribution have been obtained by Maccabee and Papworth.[20] Rohrlich and Carlson,[21] using the Møller cross section, Eq.(2), for the energy transfer in single electron-electron collisions, found that the corrections for relativistic, spin and exchange effects are practically negligible. Vavilov[22] used a finite maximum energy transfer in obtaining the energy-loss distribution of heavy charged particles. His result was a distribution in terms of two variables. However, when applied to electrons traveling short pathlengths, the Vavilov distribution reduces* to the simpler Landau distribution.

Blunck and Leisegang,[23] by including a higher order term in an expansion used in solving Landau's transformed equation, derived a method to take into account more details of atomic excitation. Their result, in the form of a correction to the Landau distribution, is given by

$$f^{*}(\Delta,s) = \frac{1}{\sqrt{2\pi}\,\sigma} \int_{-\infty}^{+\infty} f(\Delta',s)\, \exp\left[\frac{(\Delta-\Delta')^2}{2\sigma^2}\right] d\Delta' \quad . \tag{20}$$

According to Blunck and Westphal,[24] the variance of the Gaussian in Eq.(20) is given by

$$\sigma^2 = 10\,\bar{\Delta}\,Z^{4/3}\ eV^2 \quad , \tag{21}$$

where $\bar{\Delta}$ is the mean collision energy loss (in eV) for pathlength s ($\bar{\Delta} = L_c(E)s$).

---

*Differences in the large energy-loss, essentially single-scattering, tail can be minimized by truncating the Landau distribution at the appropriate maximum energy loss. The remaining differences have little practical affect, since these large energy losses are very rare.

B. Angular Deflections

1. Single Elastic Scattering

The Rutherford[25] cross section for the scattering of a non-relativistic electron by a bare nucleus of charge Ze is

$$\sigma_R(\theta) = \frac{Z^2 e^4}{p^2 v^2 (1-\cos\theta)^2} \quad . \tag{22}$$

The screening of the nuclear charge by the orbital electrons can be accounted for by replacing $(1-\cos\theta)$ with $(1-\cos\theta + 2\eta)$. From the work of Molière[26]

$$\eta = \frac{1}{4}\left(\frac{\hbar}{pa}\right)^2 \left[1.13 + 3.76\left(\frac{Ze^2/\hbar c}{\beta}\right)^2\right] \quad , \tag{23}$$

where a is the Thomas-Fermi radius

$$a = 0.885 \frac{\hbar^2}{me^2} Z^{-1/3} \quad . \tag{24}$$

The angular deflections due to inelastic scattering by the orbital electrons can be approximately accounted for by replacing Z^2 with $Z(Z + 1)$ in Eq.(22).

Mott[27] derived the cross section for scattering by an unscreened nuclear charge which displays explicitly the modifications to the non-relativistic Rutherford cross section by relativistic effects and the intrinsic spin of the electron. The Mott cross section $\sigma_M(\theta)$ is given as a slowly converging Legendre series in θ. For small angles,

$$\sigma_M(\theta) \approx \sigma_R(\theta)\left[1 + \frac{\pi}{\sqrt{2}} \frac{Ze^2\beta}{\hbar c} \cos\gamma\, (1-\cos\theta)^{1/2}\right] \quad , \tag{25}$$

where

$$\cos\gamma = \mathrm{Re}\left\{\frac{\Gamma\left(\frac{1}{2} - \frac{iZe^2/\hbar c}{\beta}\right)\Gamma\left(1 + \frac{iZe^2/\hbar c}{\beta}\right)}{\Gamma\left(\frac{1}{2} + \frac{iZe^2/\hbar c}{\beta}\right)\Gamma\left(1 - \frac{iZe^2/\hbar c}{\beta}\right)}\right\} . \tag{26}$$

Combining the Mott cross section with the screening correction and the inelastic scattering correction leads to the final form for the single scattering cross section for angular deflections

$$\sigma(\theta) = \frac{Z(Z+1)e^4}{p^2v^2(1-\cos\theta+2\eta)^2}\left\{1 + \frac{\pi}{\sqrt{2}}\frac{Ze^2\beta}{\hbar c}\cos\gamma\,(1-\cos\theta+2\eta)^{1/2} + h(\theta)\right\} , \tag{27}$$

where $h(\theta)$ represents the corrections to the small angle approximation to give $\sigma(\theta)$ for arbitrary θ and must be evaluated numerically* from $\sigma_M(\theta)/\sigma_R(\theta)$.

2. Multiple-Scattering Distribution of Angular Deflections

A solution to this problem was given by Williams[28] based on a fitting together of a Gaussian describing the central small-angle portion of the multiple scattering angular distribution and a single-scattering tail. Goudsmit and Saunderson[29] developed a theory which is exact for any angle and which can be evaluated with any single scattering law.

The Goudsmit-Saunderson distribution can be written

$$A_{GS}(\theta,s) = \sum_{l=0}^{\infty}\frac{2l+1}{2}\,e^{-sG_l}P_l(\cos\theta) , \tag{28}$$

---

*In our calculations, values of $h(\theta)$ were obtained using a FORTRAN computer code written by Dr. J. Coyne of the National Bureau of Standards.

where

$$G_\ell = \frac{2\pi N_\ell}{A} \int_{-1}^{+1} \sigma(\theta)\left[1 - P_\ell(\cos\theta)\right] d(\cos\theta) \quad . \tag{29}$$

The variation of $\sigma(\theta)$ due to energy loss along the pathlength s can be taken into account by replacing the exponent sG_ℓ in Eq.(28) with $\int_0^s G_\ell(s')ds'$. Changing the variable from s' to the fractional residual mean range

$$t = \frac{r_o - s'}{r_o} \quad , \tag{30}$$

the integral becomes

$$\int_0^s G_\ell(s')\,ds' = r_o \int_{1-s/r_o}^{1} G_\ell(t)\,dt \quad . \tag{31}$$

Spencer[30] has demonstrated that

$$G_\ell(t) \approx \frac{1+b}{t(t+b)}\, G_\ell(1) \quad , \tag{32}$$

so that

$$\int_0^s G_\ell(s')\,ds' = \frac{1+b}{b}\, r_o\, G_\ell(1)\, \ell n\left[\frac{r_o(1+b) - s}{(r_o - s)(1+b)}\right] \quad . \tag{33}$$

The constant b can be easily determined from Eq.(32) with knowledge of the G_ℓ's for the end-points of the pathlength s.

From the integral properties of Legendre polynomials it can easily be seen that the mean multiple-scattering angular deflection for pathlength s is given by

$$\langle \cos\theta \rangle_{av} = \int_{-1}^{+1} \cos\theta\, A_{GS}(\theta, s)\, d(\cos\theta) = \exp\left[-\int_0^s G_1(s')\,ds'\right] \quad . \tag{34}$$

The work of Molière[31] and Snyder and Scott[32] was done in the small angle approximation; their work and modifications to it has been reviewed by Scott.[33] The relation between the small-angle, Molière theory and that of Goudsmit and Saunderson have been discussed by Lewis[34] and Bethe,[35] who show that at small scattering angles the theory of Goudsmit and Saunderson reduces to that of Molière. In some applications the use of Molière's angular distribution may be preferred because it is more easily numerically evaluated than the distribution of Goudsmit and Saunderson.

C. Coupling of One- Variable Multiple Scattering Theories

The multiple scattering theories mentioned above are solutions to one-variable problems. The difference between pathlength and depth of penetration is disregarded; energy loss is either neglected or treated in the continuous-slowing-down approximation*; and the theories are, strictly speaking, valid only for an unbounded medium.

The solutions of the one-variable problems can be patched together or overlaid to account for both energy loss straggling and the effects of angular deflections. In order to extend Landau's theory to describe the shape of the spectrum of electrons transmitted through thicker foils, several authors[36-40] have combined the Landau energy-loss distribution with a simple foil-thickness correction derived from the work of Yang.[41] Yang obtained the distribution of actual pathlengths in a foil of a given thickness in two cases: for all particles

*In the continuous-slowing-down approximation, the energy loss per unit pathlength at every point along the electron track is assumed to be given by stopping power theory. Thus, the statistical fluctuation - straggling - in the energy loss is ignored.

regardless of angle; and only for those particles emerging at $0.^{o}$. His solution is based on the use of the small angle Gaussian approximation to multiple scattering, but can be improved by substituting in it a mean value derived from a more exact theory. A more complete approach has been used[42,43] based on the folding of the Landau and the Yang distributions. However, this method ignores the correlation between pathlength and energy-loss straggling; it cannot account for the attenuation of the incident beam due to complete absorption; and it can only be applied for the two cases treated by Yang.

These objections can be surmounted by successive convolutions of multiple scattering energy-loss and angular distributions over a series of short path segments for which the one-variable theories are valid. Performing the convolution by random sampling is the basis of Monte Carlo electron transport calculations. This approach has been rather thoroughly outlined by Berger,[9] and is distinguished by its ability to account for many types of effects (e.g. the emission and transport of secondary radiation) and to treat complex boundary conditions. The Monte Carlo calculations of Sidei et al,[44] Berger,[45-47] Mar,[48] Bishop[49] and Berger et al,[50] were done in the continuous-slowing-down approximation, convoluting only successive multiple scattering angular distributions; the work of Hebbard and Wilson,[42] Leiss et al,[51] Schneider and Cormack,[52] Perkins,[53] Meissner,[54] and Berger and colleagues[14,55-62] include also the effects of energy-loss straggling. A non-stochastic, numerical integration technique - the phase-space time evolution method - was used by Cordaro and Zucker[63] to perform the convolutions. Their calculation was done in the continuous-slowing-down approximation, but in principle it can be

extended to include energy-loss straggling.

D. Solutions of the Multi-Variable Transport Equation

Solutions of the multi-variable transport equation have been obtained in some cases. The moments method developed by Spencer[30] has been used by him[64] to calculate the depth distribution of energy deposition for a wide range of electron energies and absorber materials. The coverage has been widened by the calculations of Adawi[65] and Kessaris[66] to include 10 to 20-MeV electrons in water. Kessaris[67] has extended the moments method to obtain the spectra of electrons as a function of depth inside the medium. However, the moments method applies only to unbounded media, and calculations so far have employed the continuous-slowing-down approximation.

Using a discreet ordinates method, Bartine et al[68] have integrated the transport equation with foil boundary conditions, but with only moderate success. For low initial electron energies - below, say, 50 kev - it is feasible to accumulate the affects of successive individual interactions using a Monte Carlo method. This has been done by Maehlum,[69] Stadsnes and Maehlum,[70] Berger and Seltzer,[71] Wedde,[72] McDonald et al,[73] and McIntyre,[74] who treat single elastic collisions but assume energy loss to be continuous. Individual inelastic collisions have been included also in the work of Berger.[75]

One should also mention the application of age diffusion theory to electron transport problems. This approach has been taken in the work of Bethe et al,[76] Weymouth,[77] Roesch,[78] Meister,[79] Archard,[80] Tomlin[81] and Kanaya and Okayama[82]; Cosslett and Thomas[83] discuss its application to problems involving electrons with energies below

30 keV. As pointed out by Spencer,[30] age diffusion theory can offer only a very approximate description of electron penetration.

In summary, for electron penetration problems in bounded media for which both energy loss straggling and multiple scattering angular deflections are important, the methods which offer the most accurate solutions are the Monte Carlo, the discreet ordinates and the phase-space time evolution. Of these, the last two are more potential in nature, work having just been started using them.

III. METHOD OF CALCULATION

The path of an electron is represented by a series of short, straight line path segments, and a Monte Carlo technique is used to perform the segment-by-segment convolution of applicable multiple scattering distributions. The procedures are incorporated in the computer code ETRAN,[84] the latest version of which has been used in the present calculations. The efficacy of this method depends on two considerations: the accuracy of the underlying theoretical distributions used, and the precision of the transport model.

A. Theoretical Distributions

The limits of validity for the distributions governing energy loss in a path segment are determined primarily by the importance of the effects of the binding of the atomic electrons. The stopping power formula, Eq.(8), is not correct for electron energies not considerably greater than atomic binding energies. The use of the Møller cross section, Eq.(2), for governing the production of knock-on electrons ignores binding completely. The Landau energy-loss distribution, Eq.(19), loses its validity as the electron energy approaches atomic binding energies. Including the Blunck-Leisegang resonance broadening correction, Eq.(20), improves the Landau distribution at these lower energies; however, the width of the Gaussian correction is only approximately known, so that at very low energies or for extremely short pathlengths - for which the correction is large - the resultant distribution becomes unreliable.

A conservative estimate of the lower limit for the validity of the energy-loss formulas is the K-shell electron binding energy for

the medium. It is true that for the K-shell electrons the binding effects will be very important, but the K-shell electrons usually represent two out of many, the remainder of which have much smaller binding energies.

Since the Goudsmit-Saunderson distribution, Eq.(28), is exact, its validity depends only on that of the single-scattering cross section, Eq.(27). Molière[26] stated that his screening calculation is valid for electron kinetic energies $E \gtrsim 100Z^{4/3}$ eV. Zeitler and Olsen[85] found* that the error in the Molière approximation is of the order of $\gamma = 2Z^{4/3}(e^2/\hbar c)^2/(\beta p)$; thus an error of 5% or less implies a low energy limit of $E \gtrsim 600\ Z^{4/3}$ eV. This restriction can be relaxed in light of the fact, as shown by Scott,[33] that the multiple scattering distribution is rather insensitive to the exact value of the screening angle. As regards the separate treatment of the screening and the relativistic and spin effects used in constructing the single-scattering cross section, Zeitler and Olsen[85] pointed out that the error incurred in this factorization is also of the order of γ. The correction for inelastic deflections, replacing Z^2 by $Z(Z + 1)$, is somewhat approximate. It is correct for large angles, but fails within the screening region - for angles near zero - where it underestimates the effect. This is relatively unimportant, however, since these very small angular deflections will have little effect on the multiple scattering distribution. An additional factor for correcting for

---

*Zeitler and Olsen used a different potential than that (based on the Fermi-Thomas model) used by Molière, but they employed the same mathematical approximations.

inelastic deflections has been proposed by Fano.[86] This factor usually has little effect and has not been used in the present calculation.

The multiple scattering angular distribution describes only the statistical effects of many scatterings by individual atoms. No account is taken of quantum mechanical interference (diffraction) effects. Possible evidence of diffraction effects for electrons with energies from 60 to 100 keV has been reported[87,88] for thin metallic foils.

Based on the points brought out in the preceding paragraphs, and various comparisons with experiments, the over-all low energy limit of the calculation is estimated to be of the order of Z keV. In all of the cases considered here, the incident energy is larger than this limit. In some cases the electron histories are continued to energies below this limit, but by then the electrons are quite diffuse and little error is expected in the final results.

B. Transport Model

1. Definition of Boundary Conditions and Quantities Calculated

Electrons are incident along the z-axis, normal to the parallel-plane target ($\theta_o = 0^o$), with kinetic energy E_o. The target is assumed to have infinite extent in the x and y- directions, and only the spatial variable z is considered. The computer code is arranged so that several targets of different thickness are treated simultaneously.

The basic quantity calculated is the current of electrons transmitted (or reflected) by a target, as a function of emergent energy and angle. This quantity will be denoted as $J(E,\theta,z)$ and has the dimensions of energy^{-1} sr^{-1}, normalized to one incident electron. Other quantities, such as the distribution of energy deposition D(z)

(in units of MeV/(g/cm^2), normalized to one incident electron), are also calculated but do not constitute the chief results of this report.

Various integrals over $J(E,\theta,z)$ are useful quantities and are defined as follows:

$$A(\theta,z) = \int_0^{E_0} dE\, J(E,\theta,z) \tag{35}$$

is the angular distribution of emergent electrons (in units of sr^{-1});

$$S(E,z) = \begin{cases} 2\pi \int_0^1 d(\cos\theta)\, J(E,\theta,z) & \text{(transmission)} \\ 2\pi \int_{-1}^0 d(\cos\theta)\, J(E,\theta,z) & \text{(reflection)} \end{cases} \tag{36}$$

is the energy spectrum of emergent electrons (in dimensions of energy^{-1});

$$T_N(z) = \int_0^{E_0} dE \int_0^1 d(\cos\theta)\, J(E,\theta,z) \tag{37}$$

is the number transmission coefficient;

$$R_N(z) = \int_0^{E_0} dE \int_{-1}^0 d(\cos\theta)\, J(E,\theta,z) \tag{38}$$

is the number reflection coefficient;

$$T_E(z) = \frac{1}{E_0} \int_0^{E_0} E\,dE \int_0^1 d(\cos\theta)\, J(E,\theta,z) \tag{39}$$

is the energy transmission coefficient;

$$R_E(z) = \frac{1}{E_0} \int_0^{E_0} E\,dE \int_{-1}^0 d(\cos\theta)\, J(E,\theta,z) \tag{40}$$

is the energy reflection coefficient;

$$\Phi_A(z) = 1 - T_N(z) - R_E(z) \tag{41}$$

is the energy absorption coefficient;

$$E_{av}(z) = E_0 T_E(z) / T_N(z) \tag{42}$$

is the mean energy of the transmitted electrons; and

$$\langle \cos\theta \rangle_{av} = \frac{1}{T_N(z)} \int_0^1 d(\cos\theta)\, \cos\theta\, A(\theta, z) \tag{43}$$

is the average deflection cosine of the transmitted electrons.

2. Division of Electron Tracks into Segments

The length of the straight-line segments, or steps, are chosen so that the electron kinetic energy decreases by the factor 2^{-m} per step, on the average. That is, the size of the k^{th} step is

$$S_k = \int_{E_{k-1}}^{E_k} \frac{dE'}{L(E')} = r_0(E_{k-1}) - r_0(E_k) \quad , \tag{44}$$

where

$$E_k = 2^{-m} E_{k-1} \quad . \tag{45}$$

The logarithmic energy grid was chosen for two reasons. The Landau distribution was derived under the assumption that the single collision cross section does not change over the pathlength considered. The energy dependence of the cross section Eq.(1′) is in the multiplicative factor $1/\beta^2$. With the choice of m = 8 in Eq.(45), β^2 changes by less than 9% over any step*.

The logarithmic energy grid has the further advantage that the mean multiple-scattering angular deflection per step changes little

---

*The energy dependent parameters defining the distribution are evaluated at $(E_{k-1} + E_k)/2$ for the k^{th} step, so that the error in β^2 is, on the average, less than 5%.

from step to step. In order to reduce the mean angular deflection per step, the major steps defined by Eq.(44) are divided into n equal sub-steps. The effect of sub-step size is shown in Table 3 for a 200-keV electron beam incident on an aluminum foil. A decrease in step size beyond n = 4 does not significantly change the results if the statistical uncertainties of the entries in Table 3 are taken into account. Because the computer time needed for the Monte Carlo calculation is roughly proportional to n, the smallest value for which the final results have converged is used. For aluminum, using n = 4 results in a mean angular deflection per sub-step of about 20^{o}. The same, or smaller, mean deflection per sub-step leads to the choice of n = 2 for beryllium and mylar and n = 6 for titanium.

3. Generation of Electron Histories

The multiple scattering collision energy loss Δ for a major step* is sampled from the Landau-Blunck-Leisegang distribution, Eq.(20). The rate of energy loss is assumed to be Δ/s for purposes of estimating the electron energy along the step.

The multiple scattering angular deflection for the sub-step is sampled from the Goudsmit-Saunderson distribution, Eq.(28). The distribution is assumed to be the same for all sub-steps within a given step. The sampled polar deflection, w, is in a coordinate system whose polar axis is along the direction of motion at the beginning of the sub-step. The change in direction from θ to θ', measured with respect to the

---

*The Landau distribution is evaluated for the major step, rather than the sub-step, so that Δ is not too small. As Δ approaches the energies of the atomic electrons, the Landau distribution becomes increasingly invalid, and the energy loss depends strongly on the rather uncertain Blunck-Leisegang correction factor.

fixed z-axis, is obtained from the transformation

$$\cos\theta' = \cos\theta\cos\omega + \sin\theta\sin\omega\cos\Delta\varphi \quad , \tag{46}$$

where $\Delta\varphi$ is the azimuthal deflection in the ω-system. Electron spin-polarization is not considered, so $\Delta\varphi$ is assumed to be random.

The production of knock-on electrons, whose energies are above a specified electron cut-off energy, is sampled according to the Møller formulas, Eqs.(5) and (2). The production point is chosen randomly along the sub-step; the direction of the primary electron is taken to be θ or θ' depending on whether the production point is in the first or second half of the sub-step, respectively; and the direction of the knock-on electron is determined by the conservation of energy and momentum, Eq.(4). Because the energy loss and the angular deflection have been accounted for, on the average, in the Landau and the Goudsmit-Saunderson distributions, no change in the energy and direction of the primary is made as a result of a sampled knock-on production event. The energy, spatial, and directional coordinates of the knock-on electron are stored and used to initialize a later electron history.

The production of bremsstrahlung photons is sampled according to the cross section package described elsewhere.[14] The sampled photon energy is subtracted from the energy of the electron, thus contributing to energy-loss straggling. If the energy of the bremsstrahlung photon is greater than a chosen photon cut-off energy, the electron history is interrupted while the photon history is traced using conventional sampling techniques.[89] The photon production point and the direction of the primary electron are chosen as in the case of knock-on electrons.

The intrinsic polar angle of emission and a random relative azimuthal angle are sampled; these are then combined with the direction of the electron. The cross sections for photon interactions were taken from the tabulation of Hubbell.[90] The coordinates of photo -, Compton and pair electrons produced in the course of the photon history are saved for later electron histories, if the energy of these is greater than the electron cut-off energy. No angular deflection is applied to the primary electron in a sampled bremsstrahlung photon production event; that deflection is assumed to be included in the nuclear scattering cross section, Eq.(27), used in the Goudsmit-Saunderson distribution.

Electrons usually cross a target boundary in the middle of a sub-step. To determine the energy at crossing, the collision energy loss is re-evaluated by sampling from the Landau-Blunck-Leisegang distribution for the portion of the major step taken to the boundary. The direction at crossing is determined by sampling a deflection from an exponential approximation to the Goudsmit-Saunderson distribution for the fraction of the sub-step to the boundary. Upon crossing, a score is added to the appropriate energy and angular histogram bin for the array $J(E,\theta,z)$.

This process is repeated, step by step, until the desired number of primary histories and resultant secondary histories have been traced. A history is terminated if the electron (or photon) leaves the target or if its energy falls below the cut-off value. Also, if the residual mean range of an electron is smaller than the distance to any boundary of interest, the history is no longer followed.

The approximations inherent in the transport model mainly involve the neglect of certain correlations. The correlation of large

deflections with the production of either energetic bremsstrahlung photons or knock-on electrons is ignored. Similarly, the correlation between large energy losses by the primary electron and the appearance of energetic knock-on electrons is neglected. An additional approximation is involved in the production of a bremsstrahlung photon or knock-on electron due to the lack of detailed knowledge of the energy and direction of the primary electron within the step. The approximations could be eliminated in a single scattering Monte Carlo model, but this would result in a large increase in the already considerable amount of computer time necessary for the calculations. For example, an ETRAN calculation of the histories initiated by 10,000 1-MeV electrons incident on a thick titanium target requires about 15 minutes on an IBM 360/91.

As can be seen, the overall accuracy of the calculation depends on the interplay of a number of complicated factors. The validity of the calculational procedure is perhaps best judged through comparisons with experiments.

IV. COMPARISON WITH EXPERIMENT

Numerous comparisons of the results of ETRAN calculations with those of experiments have appeared in the literature during the past few years. Rester and Rainwater,[91] for an incident energy E_o = 1 MeV, and Berger and Seltzer,[57] for energies of 1.0, 2.66 and 8.2 MeV, compared measured and calculated distributions in energy and angle of electrons transmitted through aluminum foils. Comparisons of energy and angular distributions were also given by Lonergan et al[92] for beryllium, aluminum, and gold foils for incident energies of 4 and 8 MeV, and by Rester and Derrickson[93] for 1.0 and 2.5 MeV electrons incident on aluminum, tin, and gold targets. ETRAN results were compared to measured energy spectra of reflected electrons by Rester and Derrickson[94] for 1-MeV electrons incident on aluminum, iron, tin and gold targets. The agreement found in the above mentioned references was generally good; in a few cases large statistical fluctuations in the calculated results, due to a small sampling base, prevented conclusive findings.

Good agreement was found between measured and calculated thick target bremsstrahlung spectra by Berger and Seltzer[57] and Rester et al.[95] These two references provide comparisons for beryllium, aluminum, iron, tin, and gold for electrons incident with energies in the range from about 0.1 to 2.8 MeV. At higher energies, 10 to 40 MeV, Berger and Seltzer[14] found good agreement between calculation and measurement for tungsten targets. Although bremsstrahlung spectra are not of importance in the present work, these spectra are sensitive to the distribution in energy and angle of the primary electrons in the target, and thus offer indirect evidence as to the accuracy of the

calculation.

Distributions in depth of energy deposition have been presented in Berger et al[71] for 5 to 54 keV electrons incident on an air target; in McLaughlin and Hussman[96] for 0.1 to 3.0 MeV electrons incident on polystyrene and aluminum targets; in Rosenstein et al[97] for 2 MeV electrons incident on a polystyrene target, and in Eisen et al[98] for 2 MeV electron incident on aluminum, copper, and tin targets. Generally good agreement between calculation and experiment was found in all of these cases.

Another class of problems provides evidence of the accuracy of the calculations. The response of NaI detectors to high energy gamma rays depends on the escape of, and radiation by, electrons produced in the detector. Good agreement between calculated and experimental NaI response functions was found in Berger and Seltzer[60] for incident gamma rays with energies up to 20 MeV. A more direct test of the electron transport calculation is found in Berger et al,[58] in which calculated and experimental response functions for silicon detectors have been compared for incident electron energies of 0.25, 0.50, 0.75 and 1.00 MeV. The agreement was found to be generally good. Certain discrepancies occurring for energies of 0.25 and 0.50 MeV are possible evidence of channelling effects, presumably caused by diffraction*.

There have been few measurements of electron transmission in cases directly pertinent to the immediate problem: that of electrons with energies of a few hundred kilovolts, and foils with atomic number

---

*The silicon detectors used in the experiment referred to were highly ordered crystals. Diffraction effects, if they indeed exist in the cases mentioned, would probably be smaller in a less ordered material.

$Z \cdot 30$. The most comprehensive coverage has been for aluminum. In Figure 1, the calculated number transmission coefficient $T_N(z)$, is compared to measured values for electrons incident on aluminum targets with energies from 0.05 to 1.0 MeV. In order to greatly reduce the dependence of the results on the incident energy E_o, the number transmission is plotted not against the target thickness z, but rather the ratio z/r_o, where r_o is the mean range of the incident electrons (see Table 2). This "scaling", in addition to being intuitively appealing, has a strong theoretical basis[99,100] and has often been used in the presentation of electron penetration results. In this way, results for electrons of slightly different energies can be compared in a meaningful way.

The experimental values shown in Figure 1 were obtained by Miller and Hendricks,[101] Miller,[102] Agu et al,[103] and Horikiri et al[104] in measurements using a Faraday cup that subtended 85% or more of 2π. Failure to include the very large angle transmission events would cause the reported T_N-values to be at most 1 or 2% lower than obtained in a full 2π-measurement. The Faraday cup used by Dupouy et al[105,106] appears to subtend 80% of 2π (see Figure 1 of Reference 105). Their measured values were corrected by multiplying by $\int_0^{1.0} A(\theta,z)d(\cos\theta) / \int_{0.2}^{1.0} A(\theta,z)d(\cos\theta)$, where $A(\theta,z)$ was obtained from the Monte Carlo calculations. This correction amounted to no more than 3% in any case. Note that $T_N(z)$ attains values larger than unity due to the transmission of knock-on electron set in motion by the primary electron. Seliger[107] used a 2π Geiger counter that recorded transmission "events" in which the emergence of a primary electron and one or more associated secondary electrons resulted in a single count. Calculated results

pertaining to such a situation are also given in Figure 1. Overall, the agreement between the calculated and experimental data is good; the differences are no larger than the differences among the various sets of experimental points themselves.

The number transmission coefficient for beryllium foils is given in Figure 2. The data of Agu et al[108] fall well below those of Dupouy et al[106] and the calculated values. The rather sketchy data of Dupouy and colleagues manifest the same dependence on E_o as that of the calculated curves, and on an absolute basis the agreement is judged to be reasonably good.

The only experimental data available for titanium foils are those of Miller.[102] For E_o = 1.0 MeV, the number transmission coefficient, as a function of titanium foil thickness, is given in Figure 3. The agreement between calculation and experiment is good. The calculated curves in Figures 1, 2 and 3 were based on the analysis of 10,000 Monte Carlo histories.

In order to test the validity of the calculated energy and angular distributions of transmitted electrons, a case considered by Rester and Derrickson[93] has been re-examined*. Calculated and experimental angular distributions of transmitted electrons are given in Figure 4, energy spectra in Figure 5, for 1 MeV electrons incident on aluminum foils. Rester and Derrickson estimate their experimental error to be about 10 per cent; the statistical errors in the calculated results are about 5 per cent. The discrepancy in the energy spectra for 0.10 g/cm^2,

---

*A comparison between experimental results and those obtained with ETRAN was given by Rester and Derrickson. However, their calculations were based on 15,000 to 20,000 Monte Carlo histories, whereas 50,000 are used here.

according to a private communication from Dr. Rester, may be due to uncertainty in the numerical integration over angle of the experimental data. On the basis of these considerations, the agreement between calculation and experiment is satisfactory.

Spectra of electrons reflected from a thick aluminum foil are given in Figure 6, for E_o = 0.5 MeV. Calculated results agree well with the measurements of Jakschik and Jüngst.[109]

Calculated and experimental distributions of energy deposition as a function of depth, D(z), are given in Figure 7 for electrons incident on thick targets of beryllium, aluminum and copper. In the experiments, the electrons passed first through a vacuum window before striking the target. Huffman et al[110] used a 0.994 mg/cm^2 aluminized mylar window; Aiginger and Gonauser,[111] 3.8 mg/cm^2 aluminum; Trump et al,[112] 17.2 mg/cm^2 aluminum; Frantz,[113] 15.5 mg/cm^2 aluminum; and Agu et al,[108] 15 mg/cm^2 beryllium. A procedure suggested by Spencer was used to account for this initial penetration: If the window was of the same material as the target, its thickness was simply added to the depth in the target at which the measurement was taken. In the cases in which the window and target materials differed, an equivalent thickness of target material, one which produces the same mean deflection cosine as calculated from the Goudsmit-Saunderson distribution, was added.

Given in Figure 7 is the dimensionless quantity $r_o D(z)/E_o$, as a function of z/r_o. Plotted this way, the dependence of the distribution on E_o is minimized, and the area under the calculated histograms is $1-R_E$. Because the measurements were relative, the experimental data have been normalized so as to give the area obtained in the

calculation. The agreement between calculation and experiment is fairly good. In particular, the agreement displayed for aluminum for incident energies of 100 and 400 keV indicates that diffraction effects are not important in these cases, at least in the determination of the energy deposition distribution.

V. NEW RESULTS

Calculations were made for 100, 150, 200, 300 and 400 keV electron beams incident on beryllium, mylar, aluminum, and titanium foils. The results are based on a sample of N = 20,000 Monte Carlo histories, except in the cases of E_o = 200 keV for which N = 50,000. Table 4 gives the number and energy coefficients T_N, R_N, T_E, Φ_A, and R_E. As defined in Chapter III, T_N and R_N are the fraction of the incident electrons which are transmitted and reflected by the foil, respectively; T_E, Φ_A and R_E, when multiplied by E_o, give the energy transmitted, absorbed and reflected by the foil, respectively. The standard deviation of the T_N and R_N results is equal to $[f(1-f)/N]^{1/2}$ upon substitution of T_N or R_N-values for f.

Table 5 gives the spectral characteristics of the transmitted electrons. In addition to the mean energy of the transmitted electrons E_{av}, the most probable energy E_p and the full-width at half maximum W of the spectrum* of transmitted electrons S(E,z) are also given. The spectral width is presented in two ways: the width referred to the incident beam energy, W/E_o; and as a characteristic of the beam now available for subsequent experimental use, W/E_p.

The quantities of Tables 4 and 5 can be interpolated to other energies and foil thicknesses by plotting them vs. z/r_o. As an example, this is done in Figures 8 and 9 for titanium, where it can be seen that the residual dependence in incident energy is difficult to separate

---

*In order to obtain smooth distributions from the histogram representations, a least-squares fit of a cubic spline was made to the histogram using a method devised by Powell.[114]

from statistical fluctuations. This apparent universality is partly illusory, however, because some real residual dependence on incident energy should remain, as can be seen, for example, in Figure 2. Rather, the composite curves of Figures 8 and 9 represent the higher energy results at small values of z/r_o and lower energy results at larger values of z/r_o. The curves are useful, however, because interpolation to values of E_o and z within the ranges listed in Tables 4 and 5 places one in the correct portion of the curve. Energy spectra of transmitted electrons S(E,Z) are given in Figure 10, where the dependencies on foil thickness, incident energy and foil material are shown.

Cumulative angular distributions of transmitted electrons, $\int_{\cos\theta}^{1} A(\theta',z)d(\cos\theta')$, are given in Table 6. The fraction of incident electrons transmitted in directions within a specified cone can be obtained by multiplying the appropriate value from Table 6 by that for T_N. The angular distributions may also be scaled to facilitate interpolation with respect to E_o and z. In Figure 11, percentile cosines of the cumulative angular distribution are plotted vs. z/r_o for beryllium, mylar, aluminum, and titanium foils. As can be seen, beyond a certain value of z/r_o the shape of the angular distributions no longer changes. These equilibrium shapes are given in Figure 12 where they are compared to that due to differential angular distributions proportional to $\cos\theta$ and to $\cos^2\theta$. It appears that the equilibrium angular distributions can be closely represented by $\cos\theta\ (a + b\cos\theta)$ in agreement with the theoretical results of Bethe et al.[76] The approach to equilibrium, as well as the dependence on foil material, for the differential angular distribution $A(\theta,z)$ can be seen in Figure 13.

To a large extent the energy and angular dependence of the transmitted current can be separated, and $J(E,\theta,z)$ can be approximated by the quantity $S(E,z)A(\theta,z)/T_N(z)$. This is shown in Figure 14 for 200 keV electrons incident on a 1-mil titanium foil. The histograms are $J(E,\theta,z)$ averaged over the angular intervals $0^o \leq \theta \leq 10^o$, $30^o \leq \theta \leq 40^o$ and $60^o \leq \theta \leq 70^o$; the curves are the corresponding approximate quantities obtained using the results found in Table 4 and Figures 10 and 13. For many applications the approximation may be sufficient. It is constructed so as to be correct on the average, but it cannot account for all details. As can be seen in Figure 14, the distribution $J(E,\theta,z)$ peaks at lower energies, and is wider, for greater angles of emergence. This is due to the fact that the electrons emerging at larger angles travel, on the average, a longer pathlength. For those instances for which more detailed information is desired, tables of $J(E,\theta,z)$ in histogram form are given in the Thesis on file at the University of Maryland.

VI. COMPARISON WITH SIMPLE THEORY

The Monte Carlo calculation incorporates the multiple scattering distributions of Landau (for energy loss) and of Goudsmit and Saunderson (for angular deflections). It is of interest to determine the conditions under which the use of these two theories by themselves, without recourse to a Monte Carlo calculation, may suffice to describe electron transmission through foils.

According to Landau's theory, the most probable energy of transmitted electrons can be written

$$\frac{E_p}{E_o} = 1 - \frac{\xi}{E_o}\left\{ \ln\left[\frac{2 m c^2 \beta^2}{(1-\beta^2) I^2}\right] - \beta^2 + 0.198 \right\} . \qquad (47)$$

Eq.(47) is obtained from Eq.(17) using for the value of the most probable λ, $\lambda_p = -0.225$. The pathlength s in the definition of ξ (see Eq.(18)) is interpreted to be the foil thickness.

The predictions of Eq.(47) are compared to Monte Carlo results in Figure 15. The Monte Carlo data are from the calculations used to generate the silicon response functions which were verified experimentally in a previously mentioned comparison.[58] The Landau curves have slopes that are proportional to terms which are essentially the collision loss stopping power; plotted vs. z/r_o, the Landau values of E_p/E_o are not independent of E_o.

The full-width at half-maximum of the Landau distribution is $W_L = 4.02\ \xi$. The FWHM of the Blunck-Leisegang Gaussian correction is, $W_{BL} = (8 \ln 2)^{1/2}\sigma$, where σ is given by Eq.(21). Assuming the peak region of the Landau distribution is sufficiently Gaussian-like, the width of

the convolution of the Landau and Blunck-Leisegang distributions is $[W_L^2 + W_{BL}^2]^{1/2}$. The most probable energy and the width of the energy spectrum of transmitted electrons, obtained from these theories are compared with the Monte Carlo results for titanium foils in Figure 16. As in the case of silicon in Figure 15, the agreement is best for foil thickness that are small fractions of the mean electron range - for which the effects of multiple scattering angular deflections and energy loss are unimportant.

The mean deflection cosine obtained from the Goudsmit-Saunderson distribution is given by Eq.(34). The Goudsmit-Saunderson results pertain to the flux of electrons in an infinite medium crossing a small spherical probe in any direction, whereas the Monte Carlo results are for the current of electrons crossing the plane exit face of the foil in the forward direction only. The flux and current are related by a factor of $\cos\theta$, but for distributions which peak strongly at small angles the differences between the two will be small. The Goudsmit-Saunderson and Monte Carlo mean deflection cosines are given in Figure 17. The agreement is good for small foil thicknesses for which small angular deflections predominate.

REFERENCES

1. C. A. Fenstermacher, M. J. Nutter, W. T. Leland and K. Boyer, Appl. Phys. Lett. 20, 56 (1972).

2. H. G. Ahlstrom, G. Inglesakis, J. F. Holtzrichter, T. Kan, J. Jenson and A. C. Kolb, Appl. Phys. Lett. 21, 492 (1972).

3. V. T. Stannett and E. P. Stahel, Ann. Rev. Nucl. Sci. 21, 397 (1971); see also A. S. Hoffman, Atomic Energy Rev. 9, 347 (1971); J. R. Puig, Atomic Energy Rev. 9, 373 (1971); and A. Danno, Atomic Energy Rev. 9, 399 (1971).

4. R. D. Evans, The Atomic Nucleus, (McGraw-Hill Book Co., New York, 1955).

5. B. Rossi, High Energy Particles, (Prentice-Hall, Englewood Cliffs, New Jersey, 1952).

6. H. A. Bethe and J. Ashkin, Experimental Nuclear Physics, L. Segre, ed., Vol. I, p. 276 (John Wiley and Sons, Inc., New York, 1953).

7. U. Fano, Phys. Rev. 92, 328 (1953).

8. R. D. Birkhoff, Handbuch der Physik, S. Flugge, ed., Vol. 34, p. 53 (Springer-Verlag, Berlin, 1958).

9. M. J. Berger, Methods in Computational Physics, B. Adler, S. Fernbach and M. Rotenberg, eds., Vol. I, p. 135 (Academic Press, Inc., New York, 1963).

10. C. D. Zerby and F. L. Keller, Nucl. Sci. and Engr. 27, 190 (1967).

11. C. Møller, Ann. Physik 14, 531 (1932); see also J. M. Jauch and F. Rohrlich, The Theory of Photons and Electrons (Addison-Wesley Publishing Co., Inc., Reading, Massachusetts, 1955).

12. H. A. Bethe, Handbuch für Physik, Vol. 24/2, p. 273 (Julius Springer, Berlin, 1933).

13. R. M. Sternheimer and R. F. Peierls, Phys. Rev. B 3, 3681 (1971).

14. M. J. Berger and S. M. Seltzer, Phys. Rev. C 2, 621 (1970).

15. M. J. Berger and S. M. Seltzer, National Aeronautics and Space Administration Publ. SP-3012 (1964).

16. M. J. Berger and S. M. Seltzer, National Aeronautics and Space Administration Publ. SP-3036 (1966).

17. E. J. Williams, Proc. Roy. Soc. (London) A 125, 420 (1929).

18. L. Landau, J. Phys. USSR 8, 201 (1944).

19. W. Börsch-Supan, J. Res. U.S. National Bureau of Standards 65B, 245 (1961).

20. H. D. Maccabee and D. G. Papworth, Phys. Lett. 30A, 241 (1969).

21. F. Rohrlich and B. C. Carlson, Phys. Rev. 93, 38 (1954).

22. P. V. Vavilov, Zh. Exper. Teor. Fiz. 32, 320 (1957); translation, JETP 5, 749 (1957).

23. O. Blunck and S. Leisegang, Z. Physik 128, 500 (1950).

24. O. Blunck and K. Westphal, Z. Physik 130, 641 (1951).

25. E. Rutherford, Phil. Mag. 21, 669 (1911).

26. G. Molière, Z. Naturforsch. 2a, 133 (1947).

27. N. F. Mott, Proc. Roy. Soc. (London) A124, 425 (1929); see also J. A. Doggett and L. V. Spencer, Phys. Rev. 103, 1597 (1956).

28. E. J. Williams, Proc. Roy. Soc. (London) 169, 531 (1939); Phys. Rev. 58, 292 (1940).

29. S. Goudsmit and J. L. Saunderson, Phys. Rev. 57, 24 (1940).

30. L. V. Spencer, Phys. Rev. 98, 1597 (1955).

31. G. Molière, Z. Naturforsch. 3a, 78 (1948).

32. H. Snyder and W. T. Scott, Phys. Rev. 76, 220 (1949).

33. W. T. Scott, Rev. Mod. Phys. 35, 231 (1963).

34. H. W. Lewis, Phys. Rev. 78, 526 (1950).

35. H. A. Bethe, Phys. Rev. 89, 1256 (1953).

36. E. L. Goldwasser, F. E. Mills and A. O. Hanson, Phys. Rev. 88, 1137 (1952).

37. H. E. Hall, A. O. Hanson and D. Jamnik, Phys. Rev. 115, 633 (1959).

38. H. Breuer, Z. Physik 180, 209 (1964).

39. G. R. Davies and R. E. Jennings, J. Phys. B, 3, 804 (1970).

40. T. Tomimasu, T. Mikado, Y. Tsuchiya, S. Sugiyama and M. Chiwaki, Denshi Gijyutsu Sohgon Kenkyusho Iho (in Japanese) 35, 92 (1971).

41. C. N. Yang, Phys. Rev. 84, 599 (1951).

42. D. F. Hebbard and P. R. Wilson, Australian J. Phys. 8, 90 (1955).

43. K. J. Van Camp and V. J. Vanhuyse, Phys. Lett. 19, 504 (1965); Z. Physik 211, 152 (1968).

44. T. Sidei, T. Higasimura and K. Kinosita, Mem. Fac. Eng. Kyoto University 19, 220 (1957).

45. M. J. Berger, National Bureau of Standards Technical Note 187 (1963).

46. M. J. Berger, National Bureau of Standards Report 8678 (1965).

47. M. J. Berger, J. Nucl. Med. 12, Suppl. No. 5, 5 (1971).

48. B. W. Mar, Nucl. Sci. and Engr. 24, 193 (1966).

49. H. E. Bishop, Brit. J. Appl. Phys. 18, 703 (1967).

50. M. J. Berger, S. M. Seltzer, H. A. Eisen and J. Silverman, Trans. Amer. Nucl. Soc. 14, 887 (1971).

51. J. E. Leiss, S. Penner and C. S. Robinson, Phys. Rev. 107, 1544 (1957).

52. D. O. Schneider and D. V. Cormack, Radiation Res. 11, 418 (1959).

53. J. F. Perkins, Phys. Rev. 126, 1781 (1962).

54. G. Meissner, Z. Naturforsch. 19a, 269 (1964).

55. M. J. Berger and S. M. Seltzer, National Aeronautics and Space Administration Publ. SP-3008 (1964).

56. M. J. Berger and S. M. Seltzer, National Aeronautics and Space Administration Publ. SP-71 (1965).

57. M. J. Berger and S. M. Seltzer, National Aeronautics and Space Administration Publ. SP-169 (1968).

58. M. J. Berger, S. M. Seltzer, S. E. Chappell, J. C. Humphreys and J. W. Motz, Nucl. Instr. Methods 69, 181 (1969).

59. M. J. Berger and S. M. Seltzer, Ann. New York Acad. Sci. 161, 8 (1969).

60. M. J. Berger and S. M. Seltzer, Nucl. Instr. Methods 104, 317 (1972).

61. M. J. Berger and S. M. Seltzer, J. Atmosph. Terr. Phys. 34, 85 (1972).

62. S. M. Seltzer and M. J. Berger, Phys. Rev. C 7, 858 (1973).

63. M. C. Cordaro and M. S. Zucker, Nucl. Sci. and Engr. 45, 107 (1971).

64. L. V. Spencer, National Bureau of Standards Monograph 1 (1959).

65. I. Adawi, Phys. Rev. 107, 1476 (1957).

66. N. D. Kessaris, Radiation Res. 23, 630 (1964).

67. N. D. Kessaris, Phys. Rev. 145, 164 (1966); Radiation Res. 43, 281 (1970).

68. D. E. Bartine, R. G. Alsmiller, Jr., F. R. Mynatt, W. W. Engle, Jr. and J. Barish, Nucl. Sci. and Engr. 48, 159 (1972).

69. B. Maehlum, Norwegian Defense Res. Est. Int. Rep. E-57 (1965).

70. J. Stadsnes and B. Maehlum, Phys. Norveg. 2, 111 (1967).

71. M. J. Berger, S. M. Seltzer and K. Maeda, J. Atmosph. Terr. Phys. 32, 1015 (1970).

72. T. Wedde, Norwegian Defense Res. Est. Int. Rep. E-162 (1970).

73. I. R. McDonald, A. M. Lamki and C. F. G. Delaney, J. Phys. D 4, 1210 (1971).

74. R. W. McEntire, University of Minnesota School of Physics and Astronomy, Cosmic Physics Tech. Rep. 159 (1972).

75. M. J. Berger, Proc. 2nd Symp. on Microdosimetry, Stresa (Italy), EURATUM Publ. EUR 4452 d-f-e, p. 541 (1970).

76. H. A. Bethe, M. E. Rose and L. P. Smith, Proc. Am. Phil. Soc. 78, 573 (1938).

77. J. W. Weymouth, Phys. Rev. 84, 766 (1951).

78. W. C. Roesch, Hanford Report HW-32121 (1954).

79. H. Meister, Z. Naturforsch. 13a, 809 (1958).

80. G. D. Archard, J. Appl. Phys. 32, 1505 (1961).

81. S. G. Tomlin, Proc. Phys. Soc. 82, 465 (1963).

82. K. Kanaya and S. Okayama, J. Phys. D 5, 43 (1972).

83. J. E. Cosslett and R. N. Thomas, Brit. J. Appl. Phys. 15, 883 (1964); Brit. J. Appl. Phys. 15, 1283 (1964); Brit. J. Appl. Phys. 16, 779 (1965).

84. M. J. Berger and S. M. Seltzer, National Bureau of Standards Reports 9836 and 9837 (1968); also Computer Code Collection 107, Oak Ridge Radiation Shielding Information Center (1968).

85. E. Zeitler and H. Olsen, Phys. Rev. 136, A 1546 (1964).

86. U. Fano, Phys. Rev. 93. 117 (1954).

87. F. Lenz, Z. Naturforsch. 9a, 185 (1954).

88. W. Hilgner and J. Kessler, Z. Physik 187, 119 (1965).

89. U. Fano, L. V. Spencer and M. J. Berger, Encyclopedia of Physics, S. Flugge, ed. Vol. 38/II, p. 660 (Springer-Verlag. Berlin, 1959).

90. J. H. Hubbell, U. S. Department of Commerce Report NSRDS-NBS 29 (1969); and private communication.

91. D. H. Rester and W. J. Rainwater, Jr., J. Appl. Phys. 37, 1793 (1966).

92. J. A. Lonergan, C. P. Jupiter and G. Merkel, J. Appl. Phys. 41, 678 (1970).

93. D. H. Rester and J. H. Derrickson, J. Appl. Phys. 42, 714 (1971).

94. D. H. Rester and J. H. Derrickson, Nucl. Instr. Methods 86, 261 (1970).

95. D. H. Rester, W. E. Dance and J. H. Derrickson, J. Appl. Phys. 41, 2682 (1970).

96. W. L. McLaughlin and E. K. Hussmann, Large Radiation Sources In Industrial Processes, p. 579. Intl. Atomic Energy Agency, STI/RUB/236, Vienna (1969).

97. M. Rosenstein, H. Eisen and J. Silverman, J. Appl. Phys. 43, 3191 (1972).

98. H. Eisen, M. Rosenstein and J. Silverman, Intl. J. Appl. Radiat. Isotopes 23, 97 (1972).

99. C. H. Blanchard, Electron Physics, National Bureau of Standards Circular 527, p. 9 (1951).

100. D. Harder, Charged Particle Tracks in Liquids and Solids, Proc. 2nd L. H. Gray Conf., Cambridge, p. 160 (1969).

101. W. E. Miller and H. D. Hendricks, National Aeronautics and Space Administration Technical Note TN D-4363 (1968).

102. W. E. Miller, National Aeronautics and Space Administration Administration Technical Note TN D-5724 (1970).

103. B. N. C. Agu, T. A. Burdett and E. Matsukawa, Proc. Phys. Soc. 71, 201 (1958).

104. S. Horikiri, Y. Nakai, H. Iomo and K. Matsuda, paper presented at Jap. Phys. Soc. Annual Meeting (1959); translation, AEC-tr-6281, p. 34.

105. G. Dupouy, F. Perrier, P. Verdier and F. Arnal, Comptes rendus 258, 3655 (1964).

106. G. Dupouy, F. Perrier, P. Verdier and F. Arnal, Comptes rendus 260, 6055 (1965).

107. H. H. Seliger, Phys. Rev. 100, 1029 (1955).

108. B. N. C. Agu, T. A. Burdett and E. Matsukawa, Proc. Phys. Soc. 72, 727 (1958).

109. J. Jakschik and K. P. Jüngst, Nucl. Instr. Methods 79, 240 (1970).

110. F. N. Huffman, J. S. Cheka, B. S. Saunders, R. H. Ritchie and R. D. Birkhoff, Phys. Rev. 106, 435 (1957).

111. H. Aiginger and E. Gonauser, Atomkernenergie 13, 33 (1967).

112. J. G. Trump, R. J. Van de Graaff and R. W. Cloud, Am. J. Roentgenol. and Rad. Therapy 43, 728 (1940).

113. F. Frantz, private communication to L. V. Spencer. Data obtained from L. V. Spencer, Phys. Rev. 98, 1597 (1955).

114. M. J. D. Powell, Atomic Energy Research Establishment (Harwell, England) Report TP 307 (1967).

Table 1. Properties of foils considered in this paper.

Material	Z/A	I (eV)	ρ (g/cm^3)	Mass Thickness of 1-mil foil (mg/cm^2)
Be	0.4438	60	1.85	4.70
Mylar, $(C_{10}H_8O_4)_n$	0.5204	73	1.38	3.51
Al	0.4818	163	2.70	6.86
Ti	0.4593	247	4.50	11.43

Z/A : ratio of atomic number to atomic weight.

I : mean excitation energy, from Ref. 15.

ρ : density.

Table 2. Electron stopping power and range. Powers of ten are shown in parentheses; e.g., 5.21(-3) means 5.21×10^{-3}.

E (MeV)	Stopping Power, L(E) (MeV cm^2/g)				Mean Range[a] $r_o(E)$ (g/cm^2)			
	Be	Mylar	Al	Ti	Be	Mylar	Al	Ti
0.05	5.46	6.23	5.07	4.50	5.21(-3)	4.59(-3)	5.71(-3)	6.52(-3)
0.06	4.79	5.47	4.47	3.97	7.17(-3)	6.31(-3)	7.82(-3)	8.90(-3)
0.08	3.93	4.49	3.68	3.29	1.18(-2)	1.04(-2)	1.28(-2)	1.45(-2)
0.10	3.40	3.88	3.20	2.86	1.73(-2)	1.52(-2)	1.86(-2)	2.10(-2)
0.15	2.67	3.05	2.54	2.28	3.42(-2)	2.99(-2)	3.64(-2)	4.09(-2)
0.20	2.30	2.64	2.20	1.98	5.45(-2)	4.77(-2)	5.77(-2)	6.46(-2)
0.30	1.94	2.22	1.86	1.69	1.02(-1)	8.94(-2)	1.08(-1)	1.20(-1)
0.40	1.76	2.03	1.71	1.55	1.57(-1)	1.37(-1)	1.64(-1)	1.82(-1)
0.50	1.66	1.92	1.62	1.48	2.15(-1)	1.88(-1)	2.24(-1)	2.48(-1)
0.60	1.60	1.85	1.57	1.43	2.77(-1)	2.41(-1)	2.87(-1)	3.17(-1)
0.80	1.53	1.78	1.51	1.39	4.05(-1)	3.51(-1)	4.17(-1)	4.59(-1)
1.00	1.50	1.75	1.49	1.37	5.37(-1)	4.65(-1)	5.51(-1)	6.04(-1)

a/ c.s.d.a. range computed in the continuous-slowing-down approximation.

Table 3. Dependence of calculated electron transmission on the step-size parameter n used in the Monte Carlo model. The average fractional energy loss per step was $0.083/n$. Results are for 200-keV electrons incident on a 2-mil (13.72 mg/cm^2) aluminum foil, and are based on a sample of 20,000 Monte Carlo histories. Quantities given are: T_N, number transmission coefficient; R_N, number reflection coefficient; T_E, energy transmission coefficient; Φ_A, energy absorption coefficient; R_E, energy reflection coefficient; E_{av}/E_o, mean energy of transmitted electrons as fraction of incident energy; $\langle\cos\theta\rangle_{av}$, mean deflection cosine of transmitted electrons.

n	T_N	R_N	T_E	Φ_A	R_E	E_{av}/E_o	$\langle\cos\theta\rangle_{av}$
1	0.911	0.061	0.726	0.240	0.034	0.797	0.695
2	0.872	0.083	0.682	0.270	0.048	0.783	0.713
4	0.845	0.100	0.660	0.282	0.058	0.781	0.726
6	0.841	0.107	0.652	0.286	0.062	0.775	0.731
8	0.841	0.104	0.650	0.288	0.062	0.772	0.733
Uncertainty[a]	±0.002	±0.002	±0.004	±0.004	±0.002	±0.005	±0.004

a/ Estimated standard deviation; magnitude approximately the same for all values of n.

Table 4. Transmission, reflection and absorption of electron beams incident on beryllium, mylar, aluminum and titanium foils. Quantities given are: T_N, number transmission coefficient; R_N, number reflection coefficient; T_E, energy transmission coefficient; Φ_A, energy absorption coefficient; R_E, energy reflection coefficient.

Beryllium

Foil thickness (mils)	Foil thickness (mg/cm^2)	Incident Energy, keV 100	150	200	300	400
				T_N		
2	9.40	0.730	0.980	0.992	1.005	1.005
3	14.10	0.205	0.902	0.978	1.003	1.006
5	23.50	0.000	0.471	0.881	0.996	1.005
				R_N		
2	9.40	0.018	0.013	0.006	0.003	0.002
3	14.10	0.018	0.017	0.012	0.005	0.003
5	23.50	0.018	0.017	0.018	0.009	0.005
				T_E		
2	9.40	0.407	0.782	0.876	0.938	0.959
3	14.10	0.068	0.606	0.795	0.902	0.936
5	23.50	0.000	0.197	0.573	0.822	0.889
				Φ_A		
2	9.40	0.584	0.211	0.120	0.061	0.040
3	14.10	0.923	0.386	0.199	0.095	0.063
5	23.50	0.991	0.795	0.419	0.174	0.109
				R_E		
2	9.40	0.009	0.007	0.004	0.001	0.001
3	14.10	0.009	0.008	0.006	0.003	0.001
5	23.50	0.009	0.008	0.008	0.004	0.002

Table 4. Continued.

Mylar						
Foil thickness		Incident Energy, keV				
(mils)	(mg/cm^2)	100	150	200	300	400
				T_N		
1/4	0.88	1.002	1.003	1.003	1.002	1.002
1/2	1.76	0.998	1.003	1.004	1.004	1.004
1	3.51	0.970	1.000	1.002	1.004	1.005
				R_N		
1/4	0.88	0.001	0.000	0.000	0.000	0.000
1/2	1.76	0.005	0.001	0.001	0.001	0.001
1	3.51	0.023	0.006	0.003	0.001	0.001
				T_E		
1/4	0.88	0.965	0.982	0.988	0.994	0.996
1/2	1.76	0.920	0.964	0.977	0.988	0.992
1	3.51	0.805	0.919	0.950	0.975	0.983
				Φ_A		
1/4	0.88	0.035	0.018	0.012	0.006	0.004
1/2	1.76	0.076	0.036	0.023	0.012	0.008
1	3.51	0.182	0.078	0.048	0.025	0.017
				R_E		
1/4	0.88	0.000	0.000	0.000	0.000	0.000
1/2	1.76	0.004	0.000	0.000	0.000	0.000
1	3.51	0.013	0.003	0.002	0.000	0.000

Table 4. Continued.

Aluminum						
Foil thickness		Incident Energy, keV				
(mils)	(mg/cm^2)	100	150	200	300	400
				T_N		
1/2	3.43	0.910	0.987	0.992	1.002	1.003
1	6.86	0.602	0.918	0.968	0.997	1.004
2	13.72	0.046	0.601	0.845	0.979	0.996
				R_N		
1/2	3.43	0.076	0.018	0.008	0.005	0.002
1	6.86	0.124	0.070	0.031	0.010	0.005
2	13.72	0.125	0.118	0.100	0.030	0.014
				T_E		
1/2	3.43	0.766	0.918	0.955	0.978	0.987
1	6.86	0.393	0.766	0.880	0.949	0.969
2	13.72	0.017	0.384	0.660	0.873	0.926
				Φ_A		
1/2	3.43	0.184	0.068	0.040	0.020	0.013
1	6.86	0.536	0.189	0.098	0.044	0.029
2	13.72	0.911	0.550	0.282	0.106	0.065
				R_E		
1/2	3.43	0.050	0.014	0.005	0.002	0.000
1	6.86	0.071	0.045	0.022	0.007	0.002
2	13.72	0.072	0.066	0.058	0.021	0.009

Table 4. Continued.

Titanium						
Foil thickness		Incident Energy, keV				
(mils)	(mg/cm^2)	100	150	200	300	400
				T_N		
1/2	5.72	0.599	0.887	0.949	0.995	1.000
1	11.43	0.105	0.597	0.808	0.957	0.985
2	22.86	0.000	0.095	0.430	0.796	0.918
				R_N		
1/2	5.72	0.216	0.112	0.052	0.013	0.007
1	11.43	0.224	0.213	0.161	0.053	0.024
2	22.86	0.224	0.220	0.219	0.166	0.091
				T_E		
1/2	5.72	0.430	0.768	0.881	0.957	0.974
1	11.43	0.050	0.419	0.662	0.873	0.931
2	22.86	0.000	0.043	0.265	0.632	0.799
				Φ_A		
1/2	5.72	0.431	0.152	0.079	0.034	0.022
1	11.43	0.808	0.448	0.231	0.088	0.051
2	22.86	0.858	0.821	0.601	0.261	0.137
				R_E		
1/2	5.72	0.139	0.080	0.040	0.009	0.004
1	11.43	0.142	0.133	0.107	0.039	0.018
2	22.86	0.142	0.136	0.134	0.107	0.064

Table 5. Characteristics of the energy spectra of electrons transmitted through beryllium, mylar, aluminum and titanium foils. Quantities given are: E_{av}/E_o, mean energy as fraction of incident energy, E_p/E_o, most probable energy as fraction of incident energy; W/E_o, full-width at half-maximum as fraction of incident energy; W/E_p, full-width at half-maximum as fraction of most probable energy.

Beryllium						
Foil thickness		Incident Energy, keV				
(mils)	(mg/cm^2)	100	150	200	300	400
				E_{av}/E_o		
2	9.40	0.557	0.799	0.883	0.933	0.954
3	14.10	0.332	0.672	0.813	0.900	0.930
5	23.50		0.418	0.650	0.825	0.885
				E_p/E_o		
2	9.40	0.642	0.841	0.908	0.952	0.969
3	14.10	0.362	0.745	0.850	0.925	0.950
5	23.50		0.479	0.713	0.865	0.911
				W/E_o		
2	9.40	0.186	0.078	0.040	0.021	0.014
3	14.10	0.284	0.123	0.073	0.033	0.020
5	23.50		0.259	0.147	0.062	0.036
				W/E_p		
2	9.40	0.290	0.093	0.045	0.022	0.014
3	14.10	0.783	0.166	0.086	0.036	0.021
5	23.50		0.541	0.206	0.071	0.040

Table 5. Continued.

Foil thickness (mils)	Foil thickness (mg/cm^2)	Incident Energy, keV 100	150	200	300	400
		Mylar				
				E_{av}/E_o		
1/4	0.88	0.963	0.979	0.985	0.990	0.994
1/2	1.76	0.922	0.961	0.973	0.984	0.988
1	3.51	0.829	0.919	0.948	0.971	0.979
				E_p/E_o		
1/4	0.88	0.976	0.987	0.992	0.996	0.997
1/2	1.76	0.945	0.974	0.983	0.991	0.994
1	3.51	0.875	0.944	0.965	0.981	0.987
				W/E_o		
1/4	0.88	0.021	0.012	0.007	0.005	0.003
1/2	1.76	0.036	0.019	0.013	0.008	0.005
1	3.51	0.079	0.032	0.025	0.013	0.008
				W/E_p		
1/4	0.88	0.022	0.012	0.008	0.005	0.003
1/2	1.76	0.038	0.019	0.014	0.008	0.005
1	3.51	0.090	0.033	0.026	0.013	0.008

Table 5. Continued.

Aluminum						
Foil thickness		Incident Energy, keV				
(mils)	(mg/cm^2)	100	150	200	300	400
				E_{av}/E_o		
1/2	3.43	0.842	0.930	0.963	0.976	0.984
1	6.86	0.653	0.835	0.909	0.952	0.965
2	13.72	0.115	0.638	0.781	0.892	0.929
				E_p/E_o		
1/2	3.43	0.901	0.954	0.971	0.985	0.990
1	6.86	0.754	0.894	0.936	0.967	0.978
2	13.72	0.392	0.742	0.849	0.925	0.953
				W/E_o		
1/2	3.43	0.091	0.038	0.026	0.015	0.010
1	6.86	0.185	0.076	0.048	0.025	0.016
2	13.72	0.326	0.197	0.102	0.046	0.026
				W/E_p		
1/2	3.43	0.101	0.040	0.027	0.015	0.010
1	6.86	0.245	0.085	0.051	0.025	0.016
2	13.72	0.832	0.266	0.120	0.049	0.028

Table 5. Continued.

Titanium						
Foil thickness		Incident Energy, keV				
(mils)	(mg/cm^2)	100	150	200	300	400
				E_{av}/E_o		
1/2	5.72	0.718	0.866	0.928	0.961	0.974
1	11.43	0.476	0.702	0.819	0.912	0.945
2	22.86		0.458	0.617	0.794	0.870
				E_p/E_o		
1/2	5.72	0.821	0.920	0.953	0.976	0.984
1	11.43	0.538	0.810	0.890	0.947	0.965
2	22.86		0.504	0.724	0.873	0.920
				W/E_o		
1/2	5.72	0.183	0.074	0.044	0.023	0.018
1	11.43	0.370	0.174	0.099	0.045	0.031
2	22.86		0.359	0.237	0.102	0.060
				W/E_p		
1/2	5.72	0.223	0.080	0.046	0.023	0.018
1	11.43	0.688	0.214	0.111	0.047	0.032
2	22.86		0.713	0.327	0.116	0.065

Table 6. Cumulative angular distribution of electrons transmitted through beryllium, mylar, aluminum and titanium foils. The quantity given is the fraction of the transmitted electrons that emerge in directions between 0^{o} and θ.

Beryllium

Foil thickness (mils)	Foil thickness (mg/cm^2)	Cone Angle, θ 5^{o}	10^{o}	15^{o}	20^{o}	30^{o}	45^{o}	60^{o}
				E_o=100 keV				
2	9.40	0.012	0.050	0.111	0.189	0.378	0.659	0.863
3	14.10	0.013	0.051	0.111	0.182	0.368	0.650	0.858
				E_o=150 keV				
2	9.40	0.024	0.086	0.185	0.301	0.539	0.802	0.934
3	14.10	0.015	0.061	0.129	0.218	0.421	0.702	0.888
5	23.50	0.013	0.050	0.107	0.176	0.360	0.645	0.853
				E_o=200 keV				
2	9.40	0.034	0.130	0.269	0.420	0.693	0.912	0.977
3	14.10	0.025	0.093	0.196	0.317	0.558	0.820	0.942
5	23.50	0.014	0.056	0.122	0.208	0.404	0.691	0.880
				E_o=300 keV				
2	9.40	0.074	0.261	0.486	0.678	0.896	0.978	0.993
3	14.10	0.050	0.185	0.365	0.546	0.806	0.949	0.986
5	23.50	0.027	0.104	0.218	0.354	0.617	0.860	0.957
				E_o=400 keV				
2	9.40	0.135	0.411	0.663	0.826	0.947	0.985	0.994
3	14.10	0.071	0.255	0.481	0.675	0.897	0.979	0.994
5	23.50	0.040	0.152	0.317	0.486	0.756	0.937	0.985

Table 6. Continued.

Mylar								
Foil thickness		Cone Angle, θ						
(mils)	(mg/cm^2)	5°	10°	15°	20°	30°	45°	60°
				E_o=100 keV				
1/4	0.88	0.056	0.208	0.412	0.613	0.881	0.990	0.999
1/2	1.76	0.035	0.134	0.273	0.436	0.707	0.919	0.979
1	3.51	0.021	0.077	0.160	0.262	0.484	0.760	0.915
				E_o=150 keV				
1/4	0.88	0.113	0.395	0.678	0.866	0.986	0.997	0.999
1/2	1.76	0.064	0.222	0.430	0.630	0.893	0.991	0.998
1	3.51	0.040	0.143	0.290	0.447	0.717	0.920	0.980
				E_o=200 keV				
1/4	0.88	0.175	0.545	0.827	0.953	0.996	0.997	0.999
1/2	1.76	0.092	0.320	0.581	0.786	0.966	0.996	0.998
1	3.51	0.065	0.240	0.446	0.632	0.857	0.962	0.988
				E_o=300 keV				
1/4	0.88	0.327	0.793	0.970	0.995	0.997	0.998	0.999
1/2	1.76	0.179	0.542	0.828	0.955	0.995	0.996	0.998
1	3.51	0.096	0.325	0.586	0.789	0.968	0.996	0.998
				E_o=400 keV				
1/4	0.88	0.449	0.904	0.992	0.996	0.996	0.997	0.999
1/2	1.76	0.257	0.692	0.931	0.987	0.996	0.997	0.998
1	3.51	0.137	0.447	0.733	0.902	0.991	0.996	0.998

Table 6. Continued.

Foil thickness (mils)	Foil thickness (mg/cm^2)	Cone Angle, θ 5°	10°	15°	20°	30°	45°	60°
				Aluminum				
				E_o=100 keV				
1/2	3.43	0.013	0.052	0.112	0.191	0.381	0.654	0.855
1	6.86	0.010	0.038	0.087	0.152	0.317	0.591	0.816
2	13.72	0.011	0.041	0.084	0.150	0.314	0.605	0.815
				E_o=150 keV				
1/2	3.43	0.022	0.088	0.186	0.305	0.560	0.826	0.943
1	6.86	0.013	0.052	0.112	0.190	0.374	0.645	0.849
2	13.72	0.011	0.039	0.090	0.158	0.320	0.593	0.821
				E_o=200 keV				
1/2	3.43	0.034	0.128	0.262	0.415	0.694	0.915	0.977
1	6.86	0.018	0.071	0.152	0.255	0.480	0.757	0.909
2	13.72	0.011	0.044	0.097	0.165	0.339	0.615	0.834
				E_o=300 keV				
1/2	3.43	0.091	0.305	0.528	0.707	0.894	0.970	0.989
1	6.86	0.041	0.150	0.302	0.462	0.719	0.910	0.973
2	13.72	0.020	0.077	0.164	0.267	0.487	0.749	0.907
				E_o=400 keV				
1/2	3.43	0.080	0.296	0.548	0.756	0.954	0.997	0.999
1	6.86	0.050	0.197	0.381	0.569	0.826	0.958	0.988
2	13.72	0.025	0.097	0.209	0.343	0.611	0.859	0.953

Table 6. Continued.

Titanium								
Foil thickness		Cone Angle, θ						
(mils)	(mg/cm^2)	5°	10°	15°	20°	30°	45°	60°
				E_o=100 keV				
1/2	5.72	0.009	0.035	0.078	0.141	0.301	0.573	0.803
1	11.43	0.011	0.039	0.087	0.145	0.314	0.583	0.821
				E_o=150 keV				
1/2	5.72	0.012	0.047	0.103	0.172	0.346	0.624	0.831
1	11.43	0.011	0.040	0.084	0.149	0.304	0.572	0.808
2	22.86	0.009	0.036	0.077	0.143	0.309	0.572	0.802
				E_o=200 keV				
1/2	5.72	0.016	0.063	0.136	0.226	0.427	0.699	0.880
1	11.43	0.010	0.041	0.088	0.155	0.319	0.588	0.814
2	22.86	0.010	0.038	0.084	0.147	0.307	0.577	0.807
				E_o=300 keV				
1/2	5.72	0.031	0.116	0.243	0.385	0.637	0.863	0.956
1	11.43	0.014	0.057	0.125	0.211	0.414	0.698	0.881
2	22.86	0.011	0.040	0.090	0.155	0.322	0.588	0.810
				E_o=400 keV				
1/2	5.72	0.042	0.155	0.311	0.481	0.751	0.936	0.983
1	11.43	0.022	0.089	0.188	0.302	0.539	0.797	0.929
2	22.86	0.012	0.048	0.102	0.180	0.364	0.634	0.841

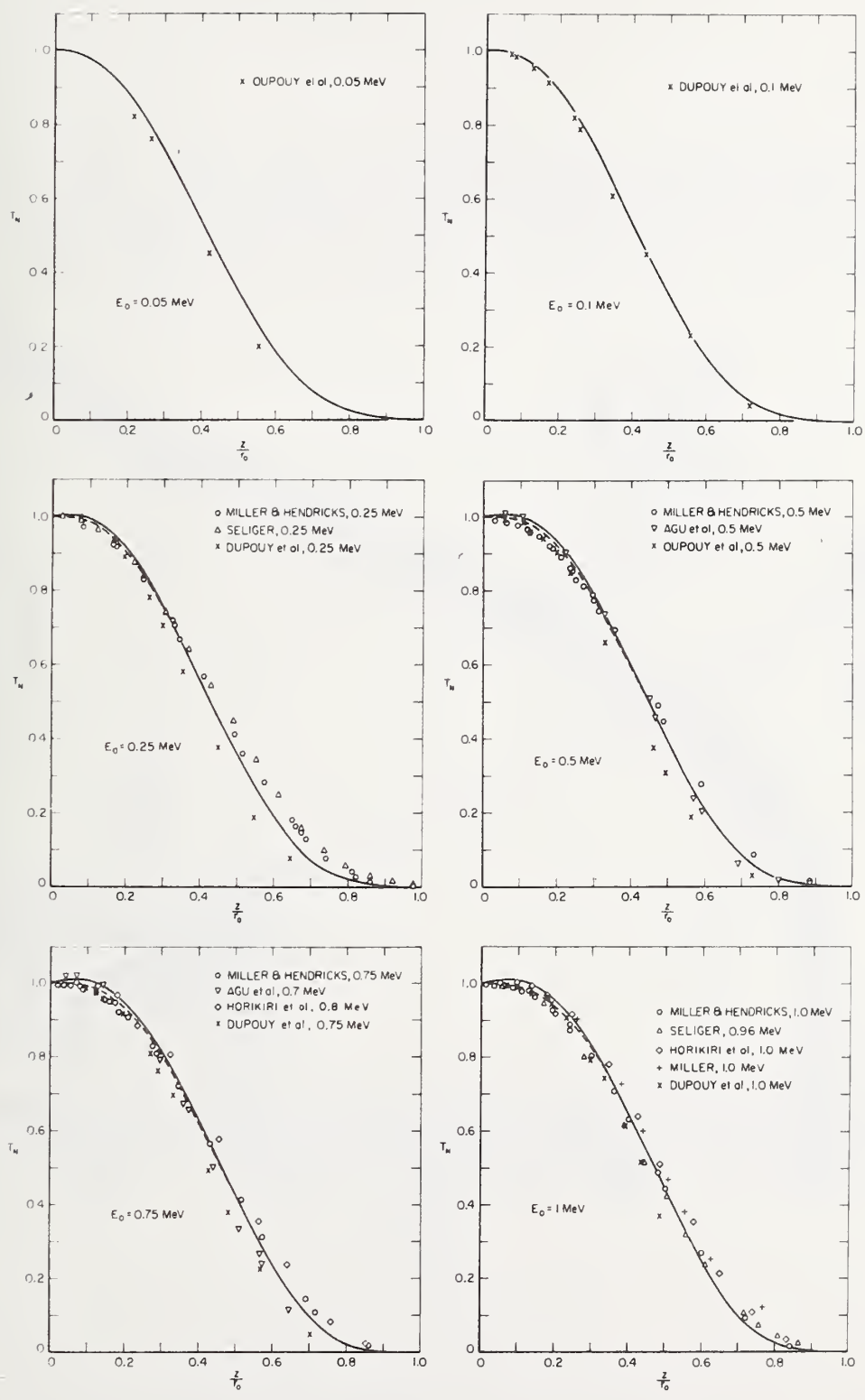
x OUPOUY et al, 0.05 MeV
E0 = 0.05 MeV
x DUPOUY et al, 0.1 MeV
E0 = 0.1 MeV
o MILLER & HENDRICKS, 0.25 MeV
Δ SELIGER, 0.25 MeV
x DUPOUY et al, 0.25 MeV
E0 = 0.25 MeV
o MILLER & HENDRICKS, 0.5 MeV
▽ ΔGU et al, 0.5 MeV
x OUPOUY et al, 0.5 MeV
E0 = 0.5 MeV
o MILLER & HENDRICKS, 0.75 MeV
▽ ΔGU et al, 0.7 MeV
◇ HORIKIRI et al, 0.8 MeV
x DUPOUY et al, 0.75 MeV
E0 = 0.75 MeV
o MILLER & HENDRICKS, 1.0 MeV
Δ SELIGER, 0.96 MeV
◇ HORIKIRI et al, 1.0 MeV
+ MILLER, 1.0 MeV
x DUPOUY et al, 1.0 MeV
E0 = 1 MeV
T_N
z/r0

Figure 1

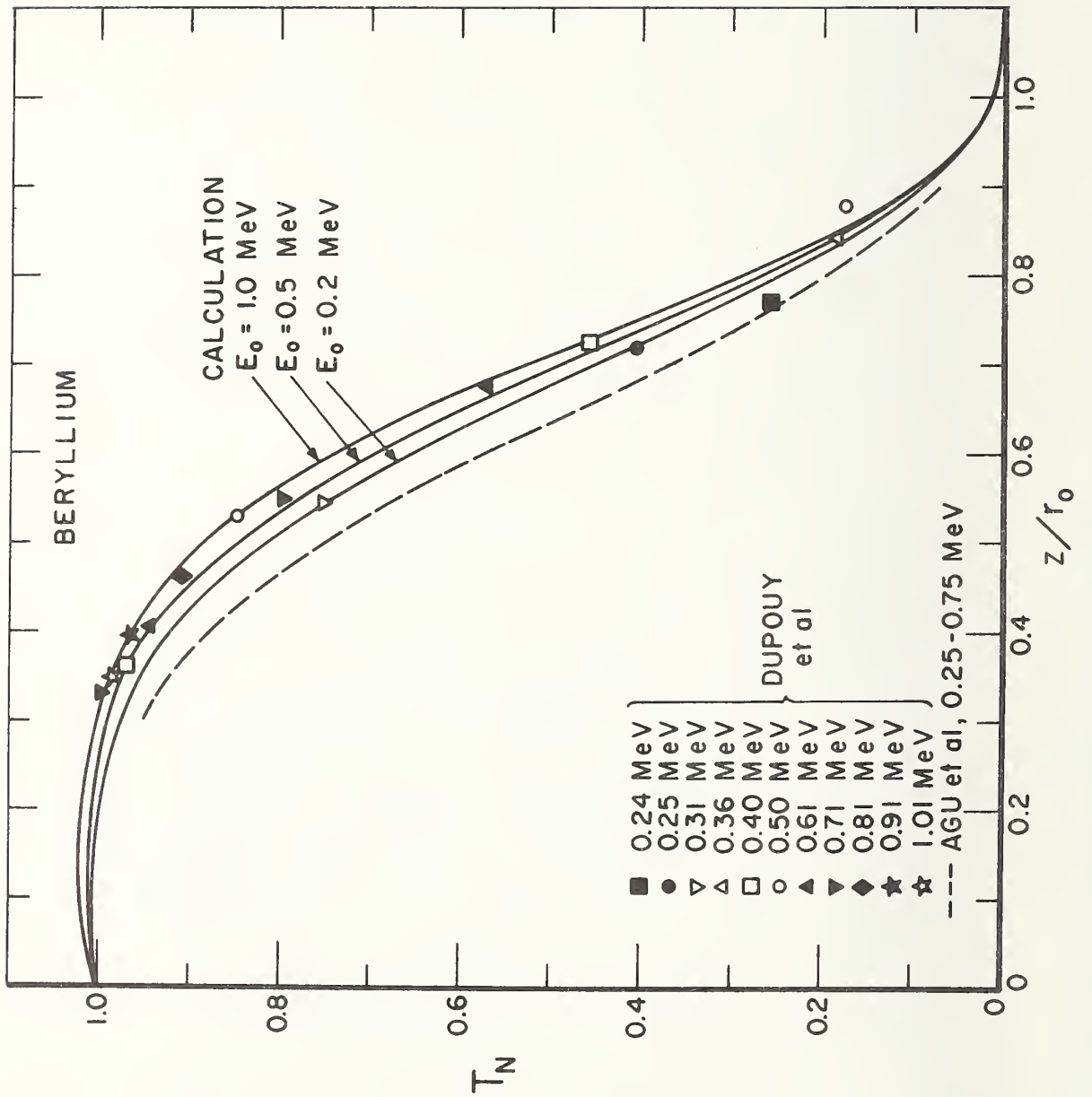
BERYLLIUM
CALCULATION
E_o = 1.0 MeV
E_o = 0.5 MeV
E_o = 0.2 MeV
DUPOUY et al
0.24 MeV
0.25 MeV
0.31 MeV
0.36 MeV
0.40 MeV
0.50 MeV
0.61 MeV
0.71 MeV
0.81 MeV
0.91 MeV
1.01 MeV
AGU et al, 0.25-0.75 MeV
T_N
z/r_o
0
0.2
0.4
0.6
0.8
1.0

Figure 2

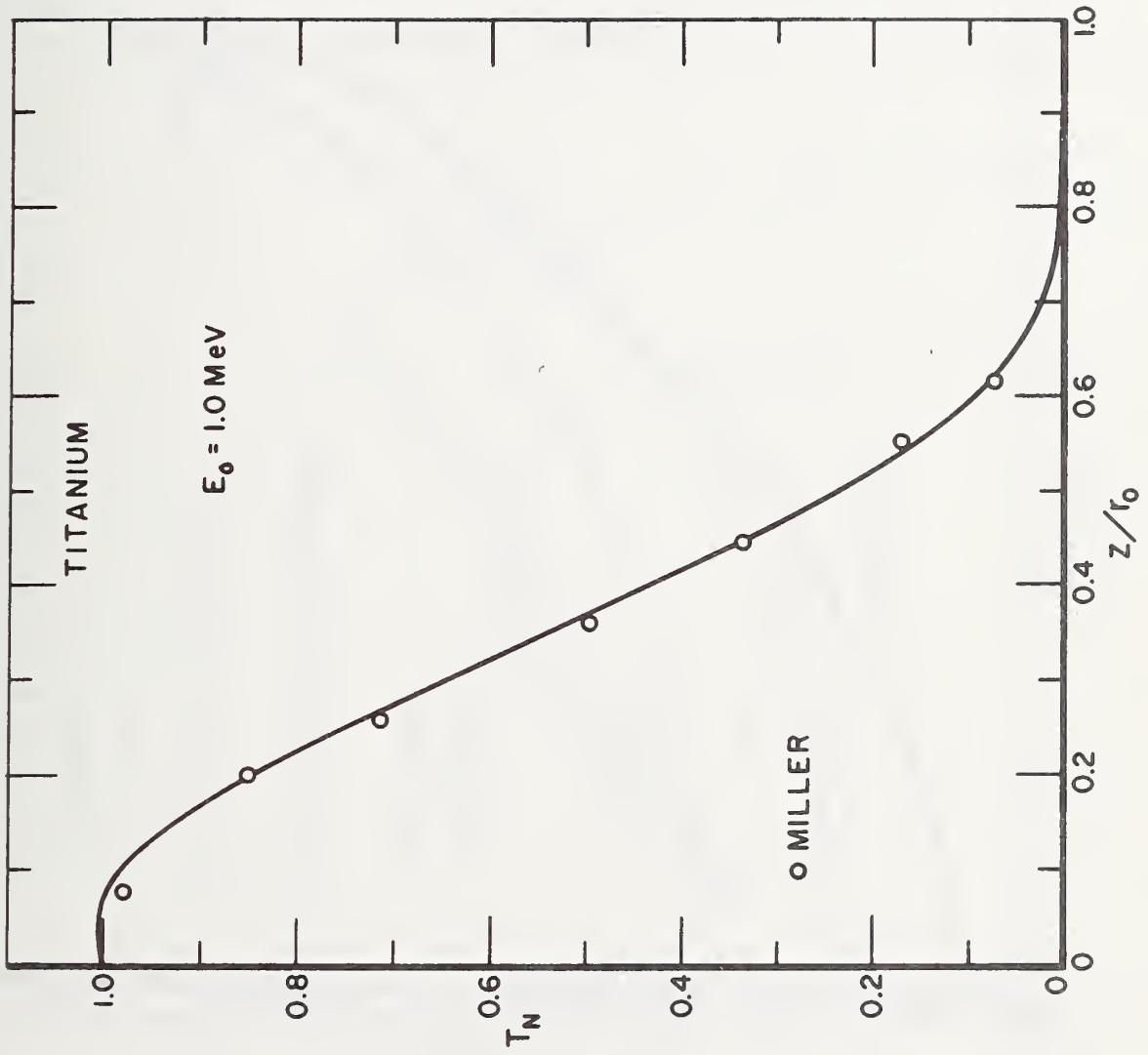

Figure 3

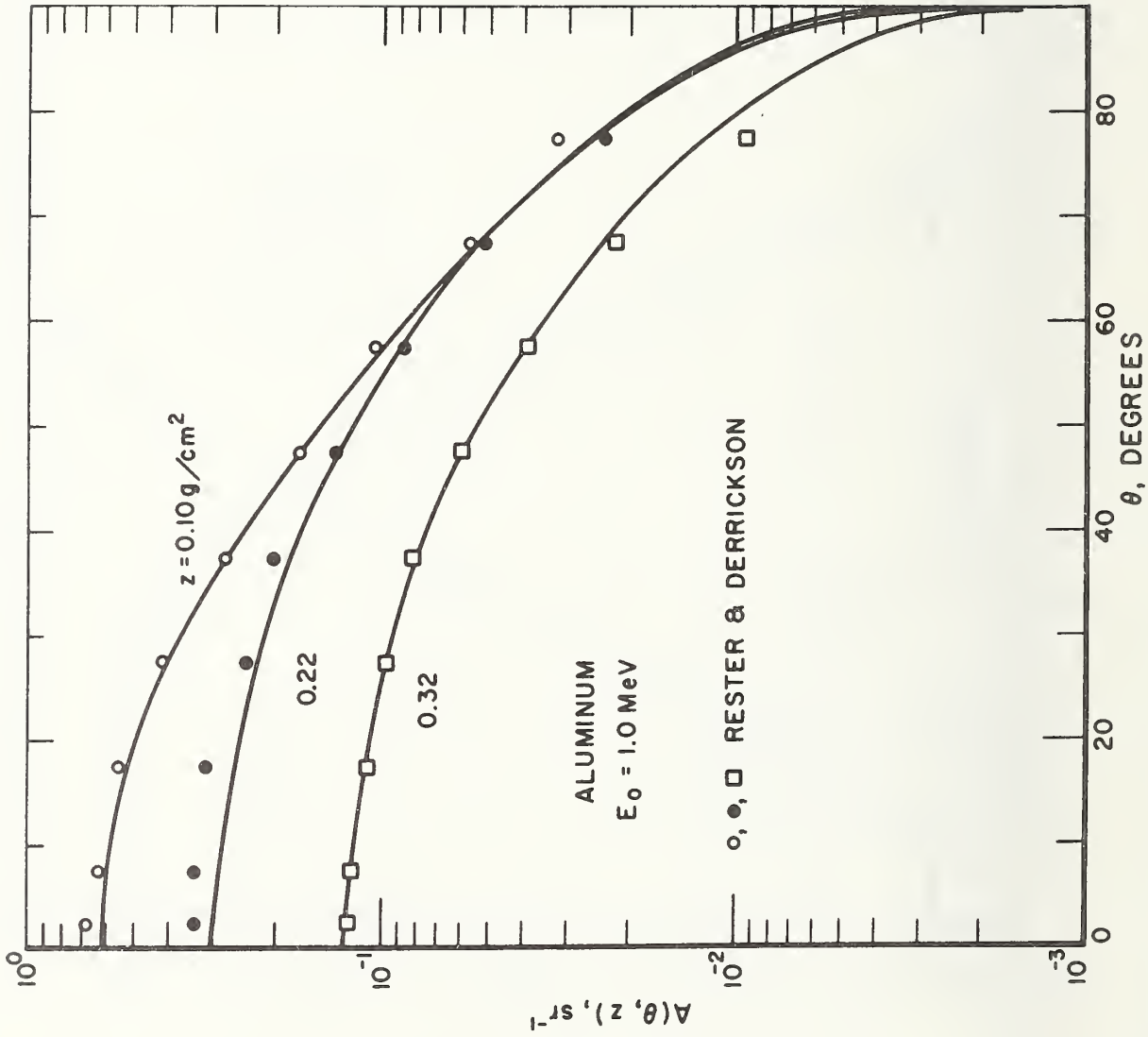
z = 0.10 g/cm²
0.22
0.32
ALUMINUM
E₀ = 1.0 MeV
o, ●, □ RESTER & DERRICKSON
θ, DEGREES
A(θ, z), sr⁻¹
10⁰
10⁻¹
10⁻²
10⁻³
0
20
40
60
80

Figure 4

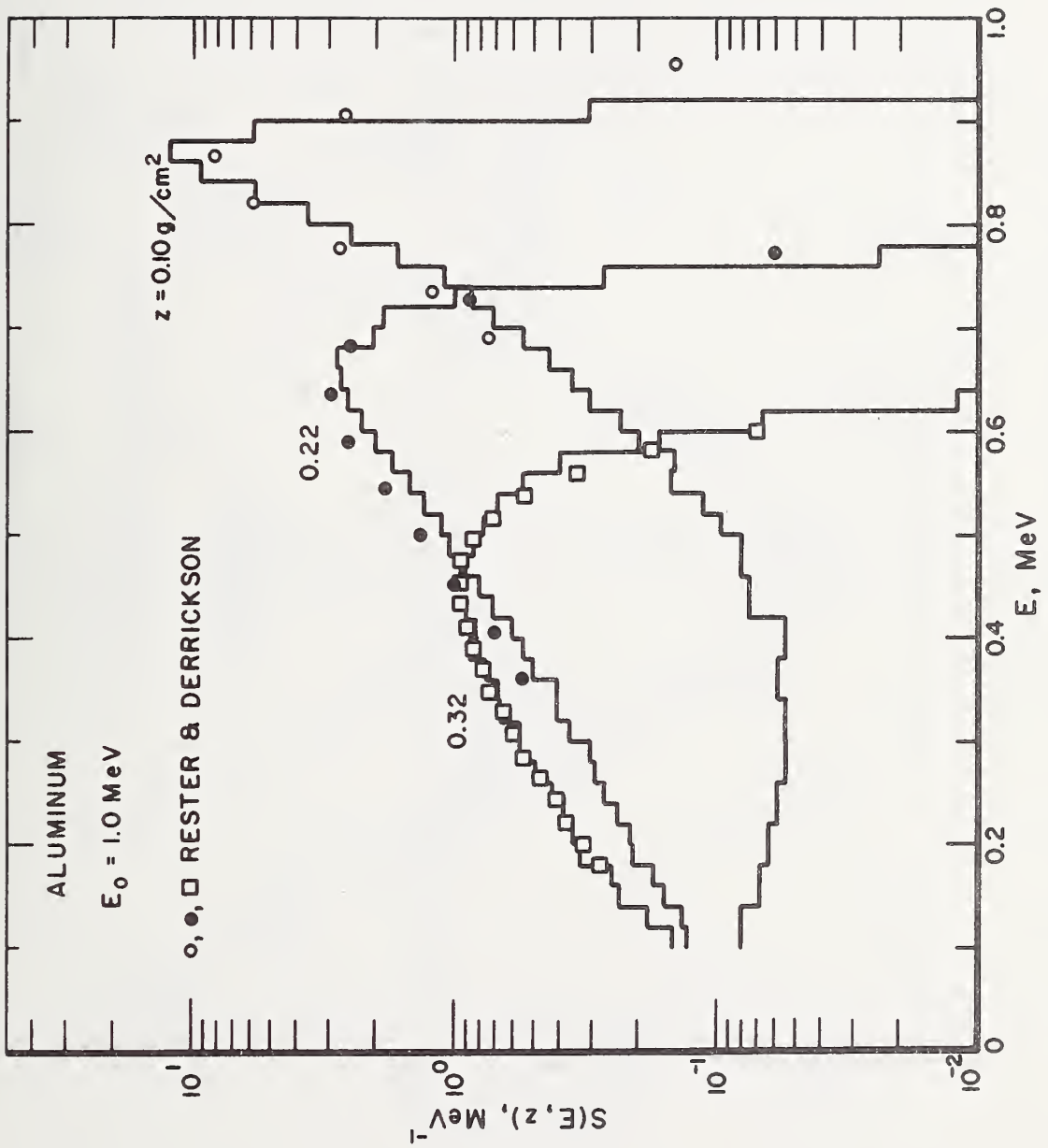
ALUMINUM
E_0 = 1.0 MeV
o, ●, □ RESTER & DERRICKSON
z = 0.10 g/cm²
0.22
0.32
S(E, z), MeV⁻¹
E, MeV
10¹
10⁰
10⁻¹
10⁻²
0
0.2
0.4
0.6
0.8
1.0

Figure 5

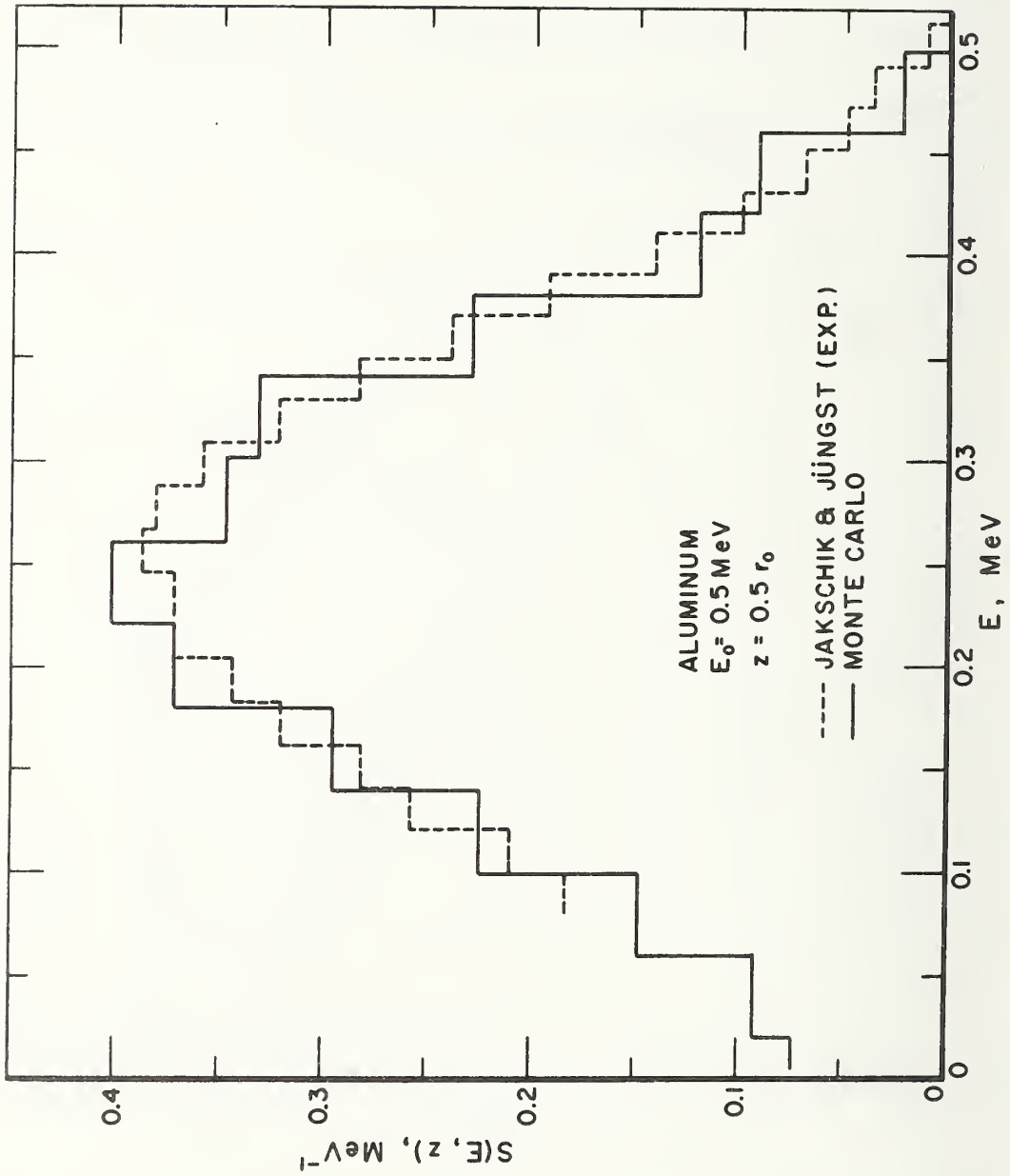
ALUMINUM
E_o= 0.5 MeV
z = 0.5 r_o
---- JAKSCHIK & JÜNGST (EXP.)
—— MONTE CARLO
S(E, z), MeV^{-1}
E, MeV
0
0.1
0.2
0.3
0.4
0.5

Figure 6

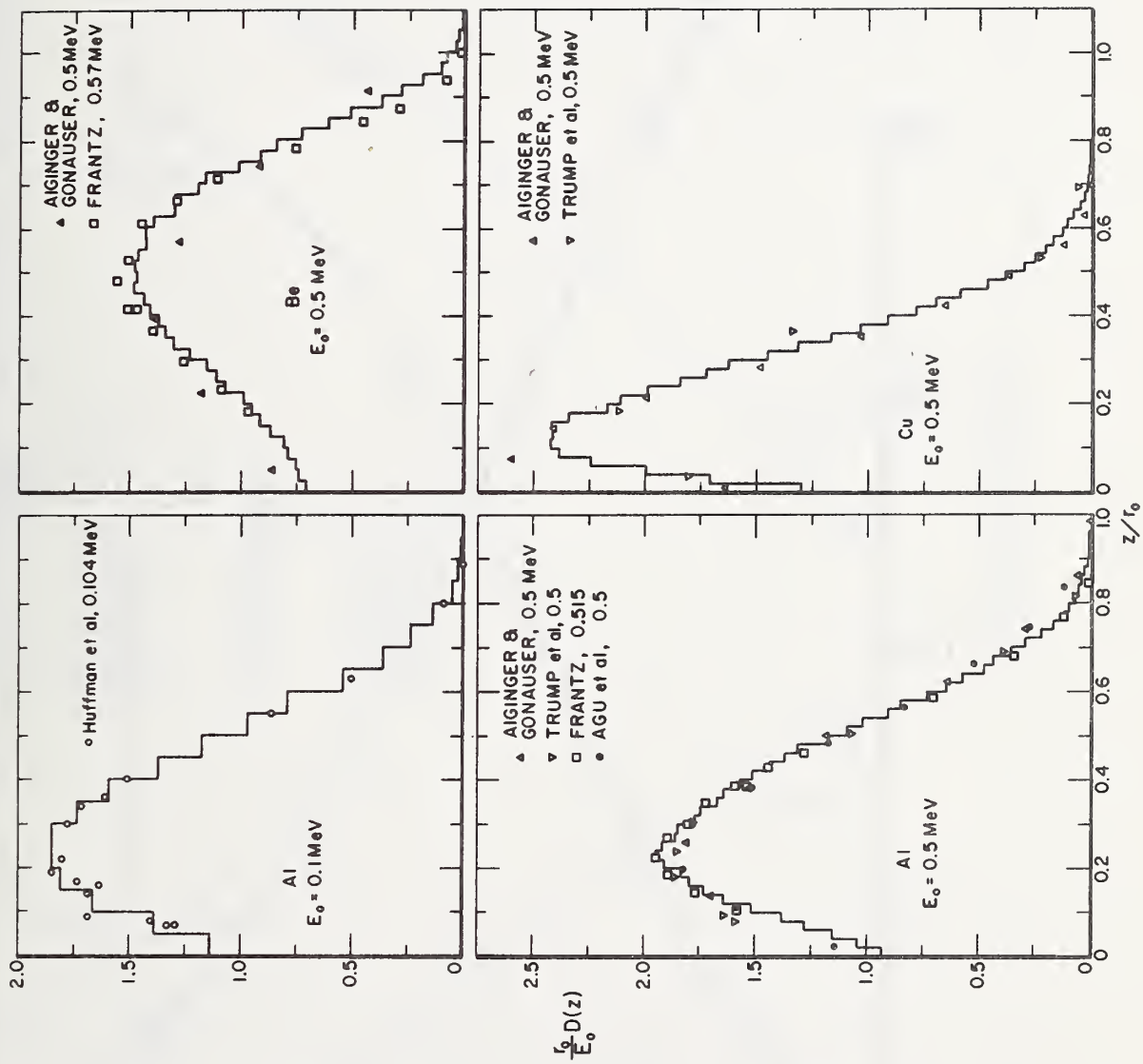
AIGINGER & GONAUSER, 0.5MeV
FRANTZ, 0.57MeV
Be
E₀ = 0.5 MeV
Huffman et al, 0.104 MeV
Al
E₀ = 0.1 MeV
AIGINGER & GONAUSER, 0.5 MeV
TRUMP et al, 0.5 MeV
Cu
E₀ = 0.5 MeV
AIGINGER & GONAUSER, 0.5 MeV
TRUMP et al, 0.5
FRANTZ, 0.515
AGU et al, 0.5
Al
E₀ = 0.5 MeV
r₀/E₀ D(z)
z/r₀

Figure 7

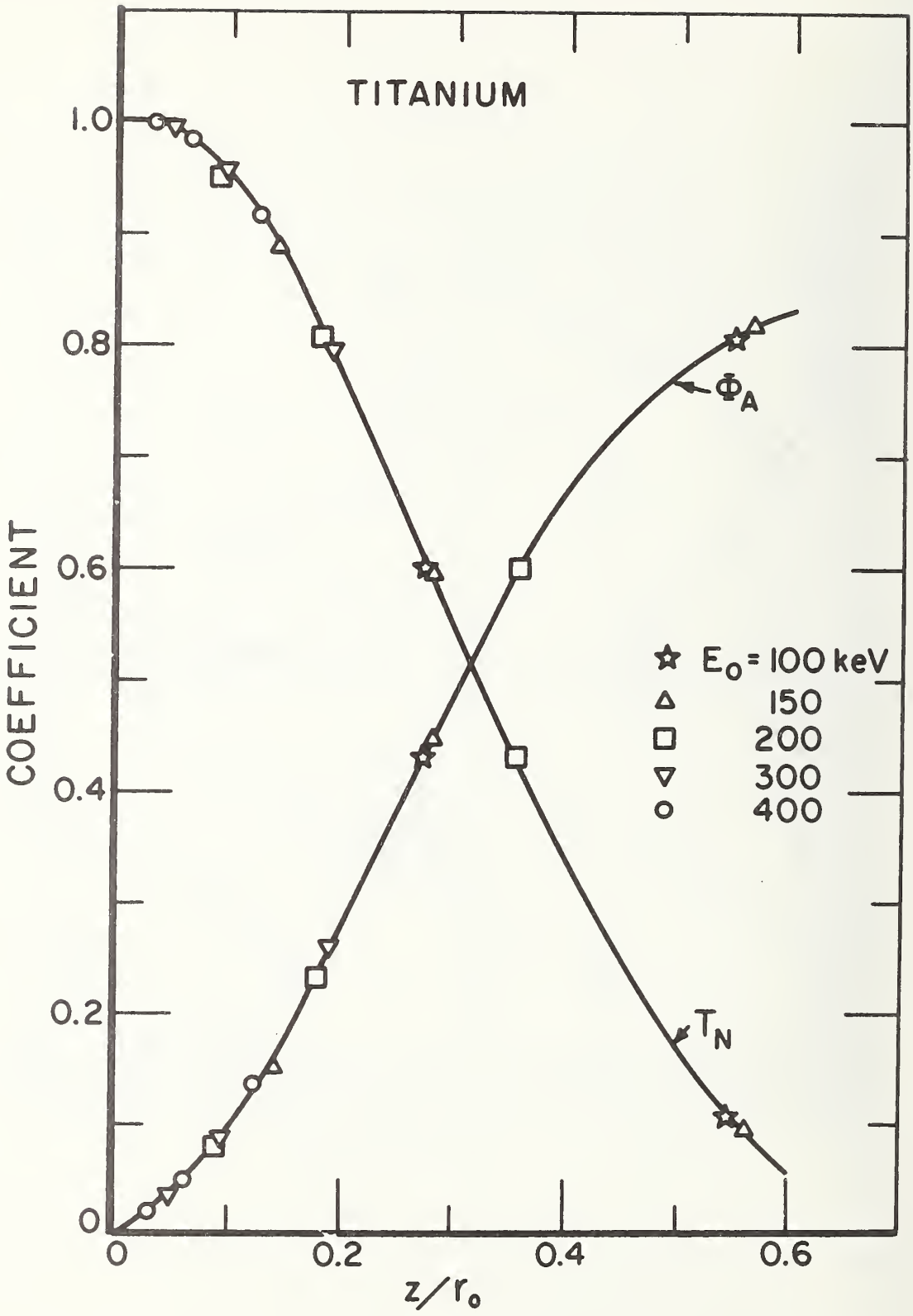
TITANIUM
COEFFICIENT
1.0
0.8
0.6
0.4
0.2
0
0
0.2
0.4
0.6
z/r₀
Φ_A
T_N
E₀ = 100 keV
150
200
300
400

Figure 8

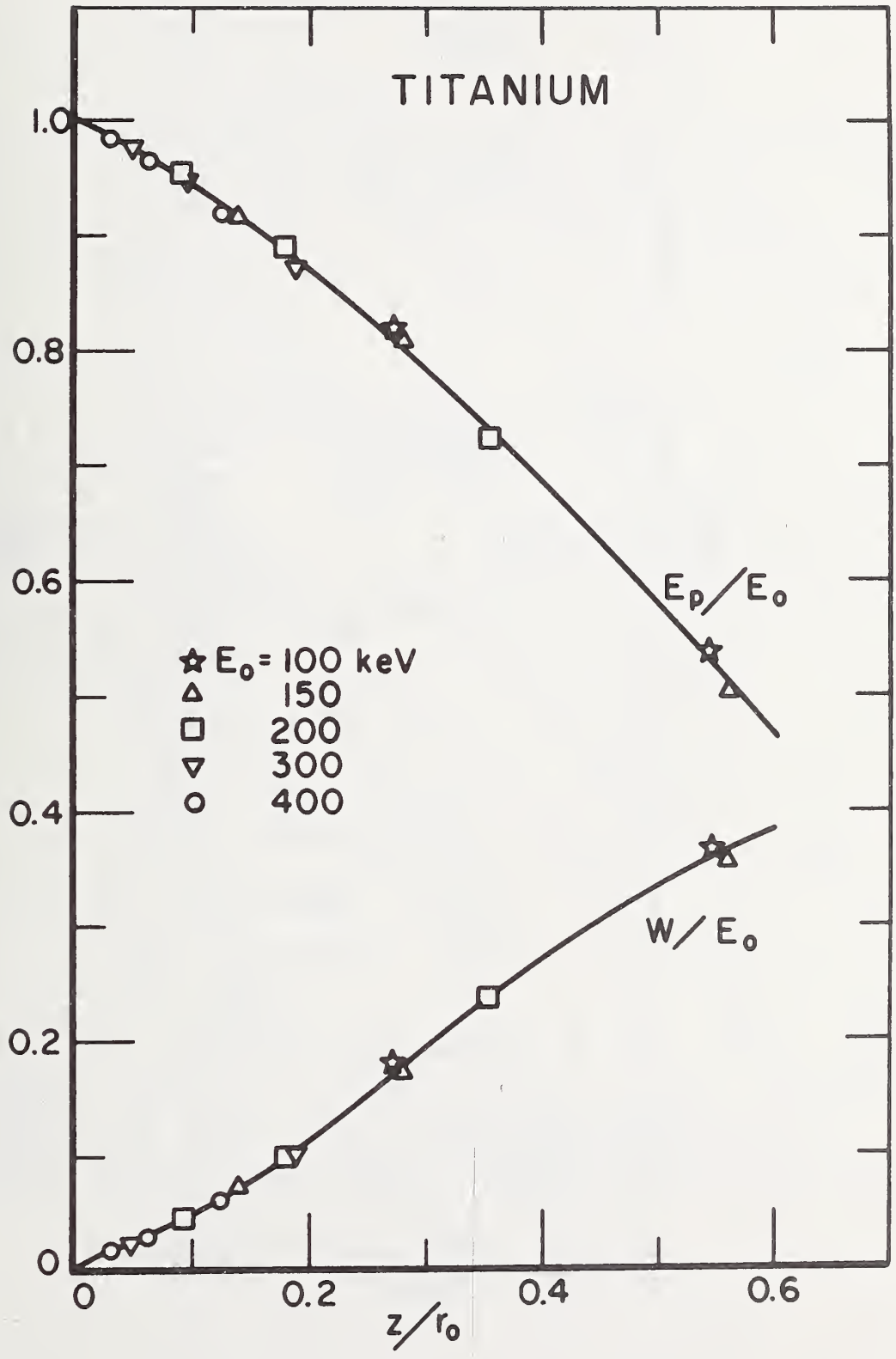
TITANIUM
1.0
0.8
0.6
0.4
0.2
0
0
0.2
0.4
0.6
z/r0
Ep/E0
W/E0
E0 = 100 keV
150
200
300
400

Figure 9

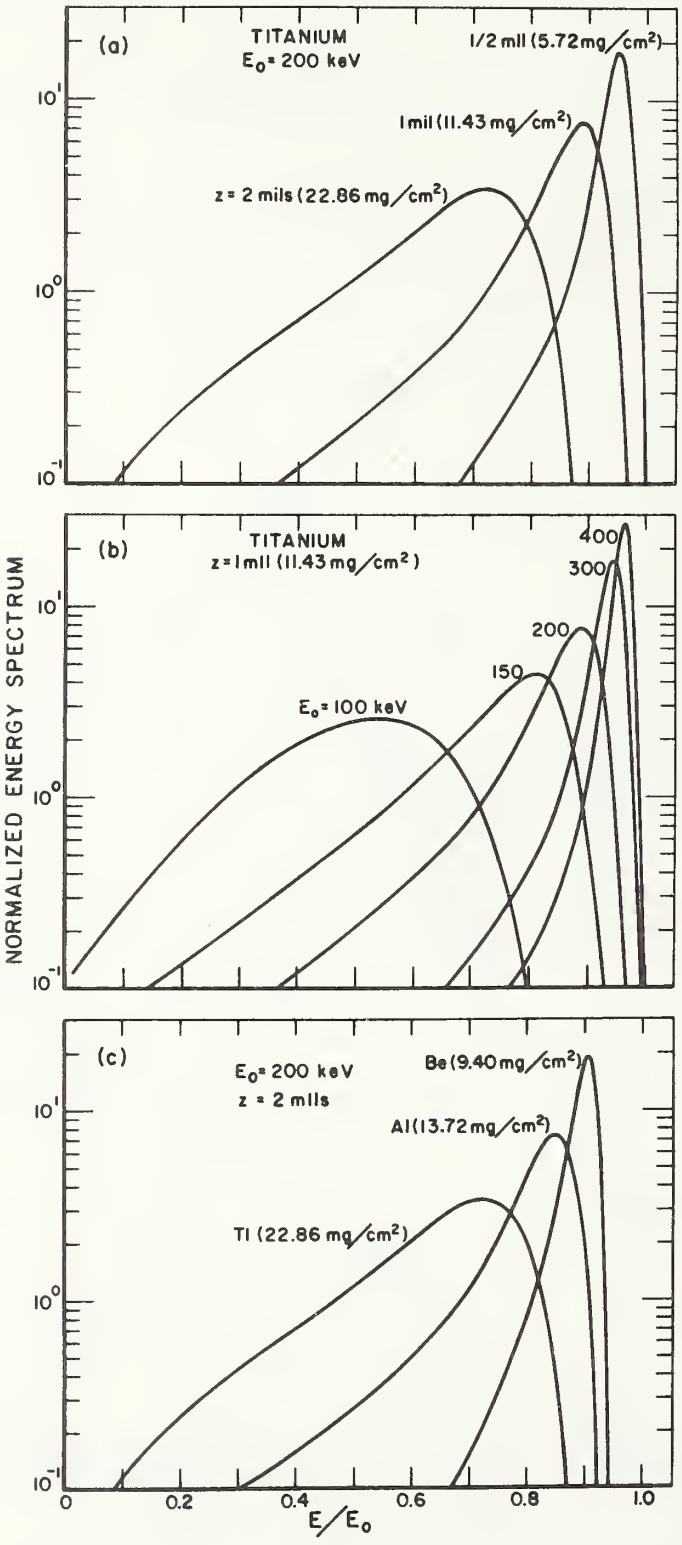
(a)
TITANIUM
E_0 = 200 keV
1/2 mil (5.72 mg/cm²)
1 mil (11.43 mg/cm²)
z = 2 mils (22.86 mg/cm²)
(b)
TITANIUM
z = 1 mil (11.43 mg/cm²)
400
300
200
150
E_0 = 100 keV
NORMALIZED ENERGY SPECTRUM
(c)
E_0 = 200 keV
z = 2 mils
Be (9.40 mg/cm²)
Al (13.72 mg/cm²)
Tl (22.86 mg/cm²)
0
0.2
0.4
0.6
0.8
1.0
E/E₀

Figure 10

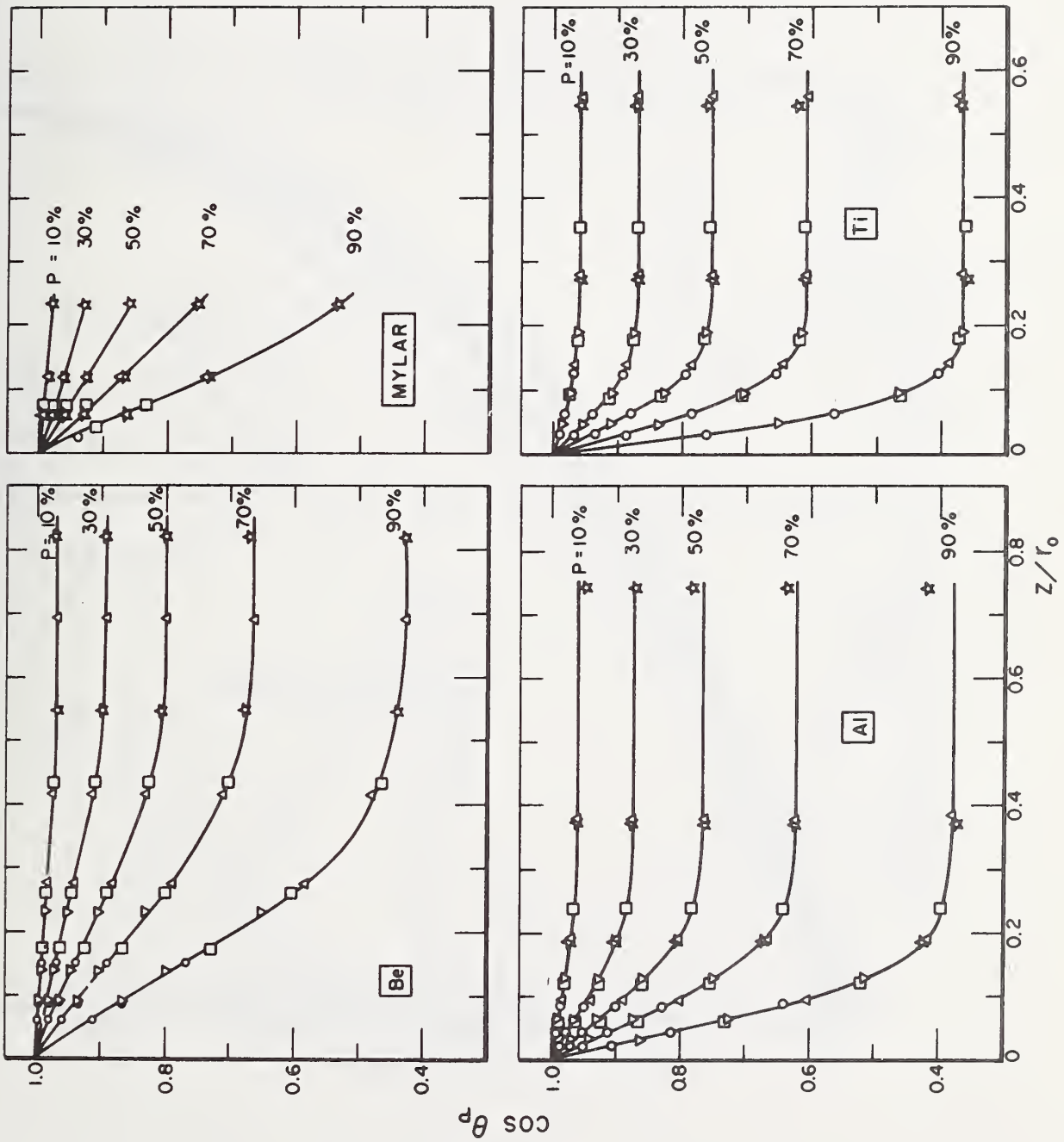

Figure 11

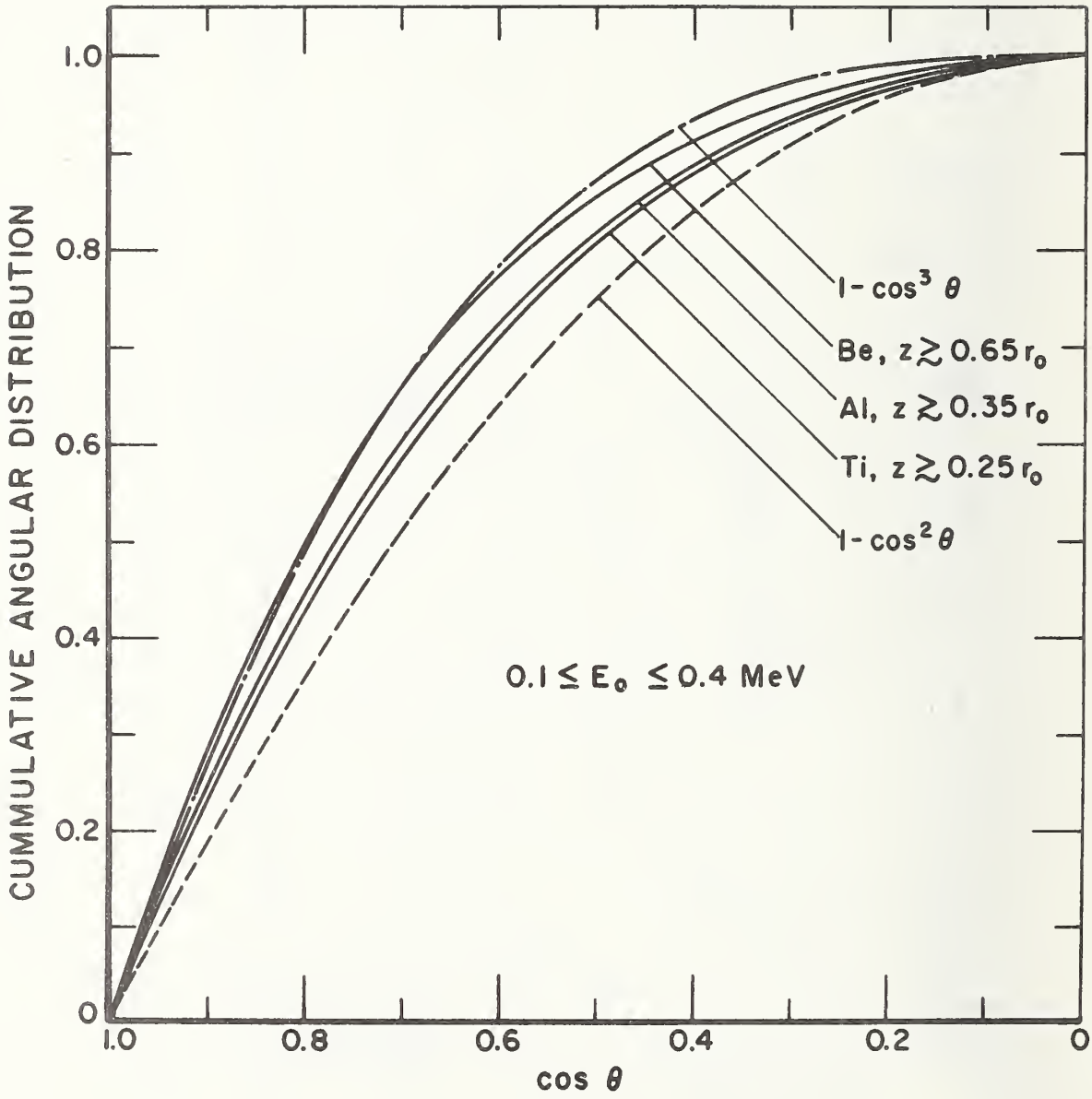
CUMMULATIVE ANGULAR DISTRIBUTION
1.0
0.8
0.6
0.4
0.2
0
1.0
0.8
0.6
0.4
0.2
0
cos θ
1 - cos³ θ
Be, z ≳ 0.65 r₀
Al, z ≳ 0.35 r₀
Ti, z ≳ 0.25 r₀
1 - cos² θ
0.1 ≤ E₀ ≤ 0.4 MeV

Figure 12

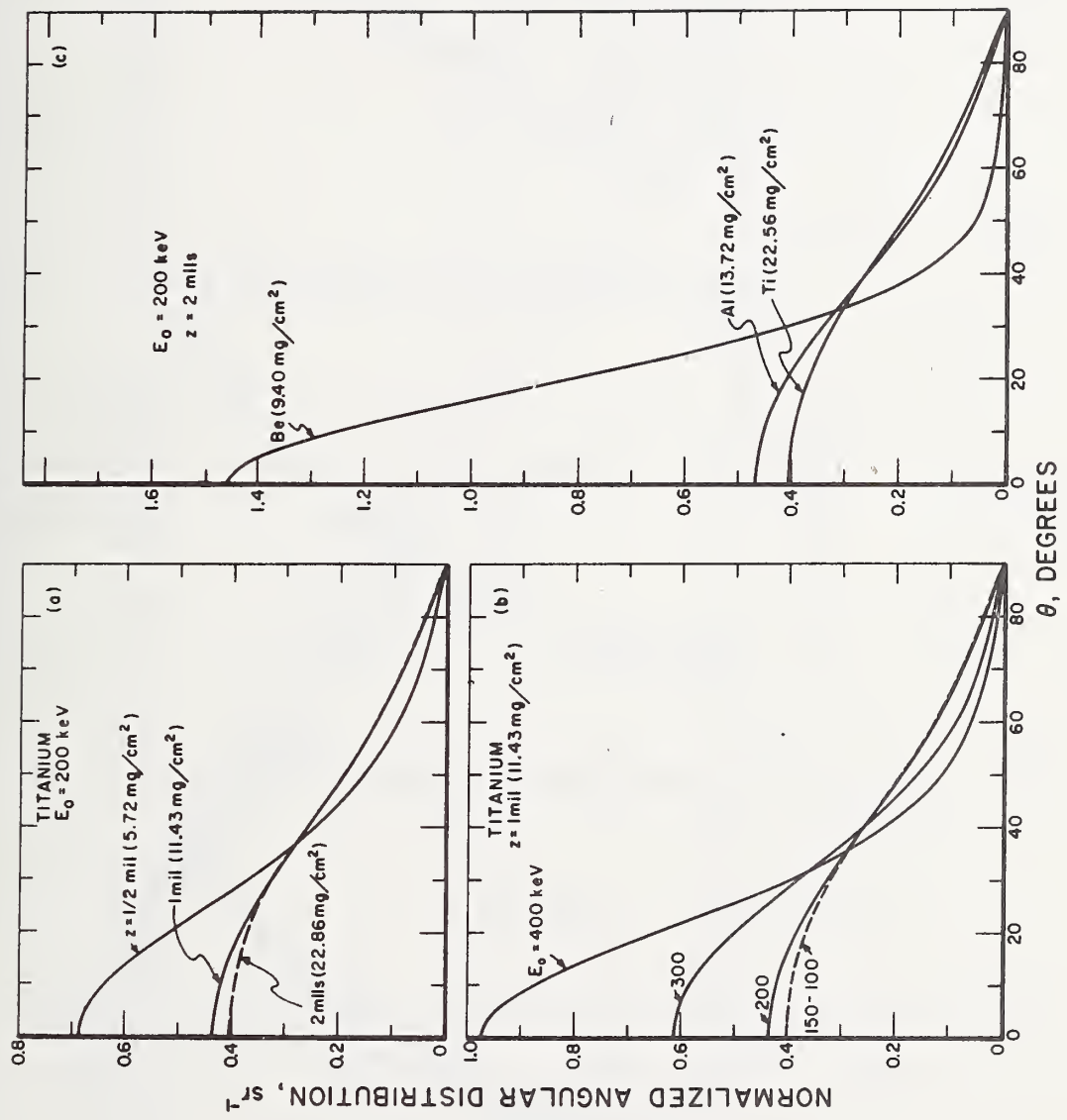
NORMALIZED ANGULAR DISTRIBUTION, sr⁻¹
θ, DEGREES
(a)
TITANIUM
E₀ = 200 keV
z = 1/2 mil (5.72 mg/cm²)
1 mil (11.43 mg/cm²)
2 mils (22.86 mg/cm²)
(b)
TITANIUM
z = 1 mil (11.43 mg/cm²)
E₀ = 400 keV
300
200
150 - 100
(c)
E₀ = 200 keV
z = 2 mils
Be (9.40 mg/cm²)
Al (13.72 mg/cm²)
Ti (22.56 mg/cm²)

Figure 13

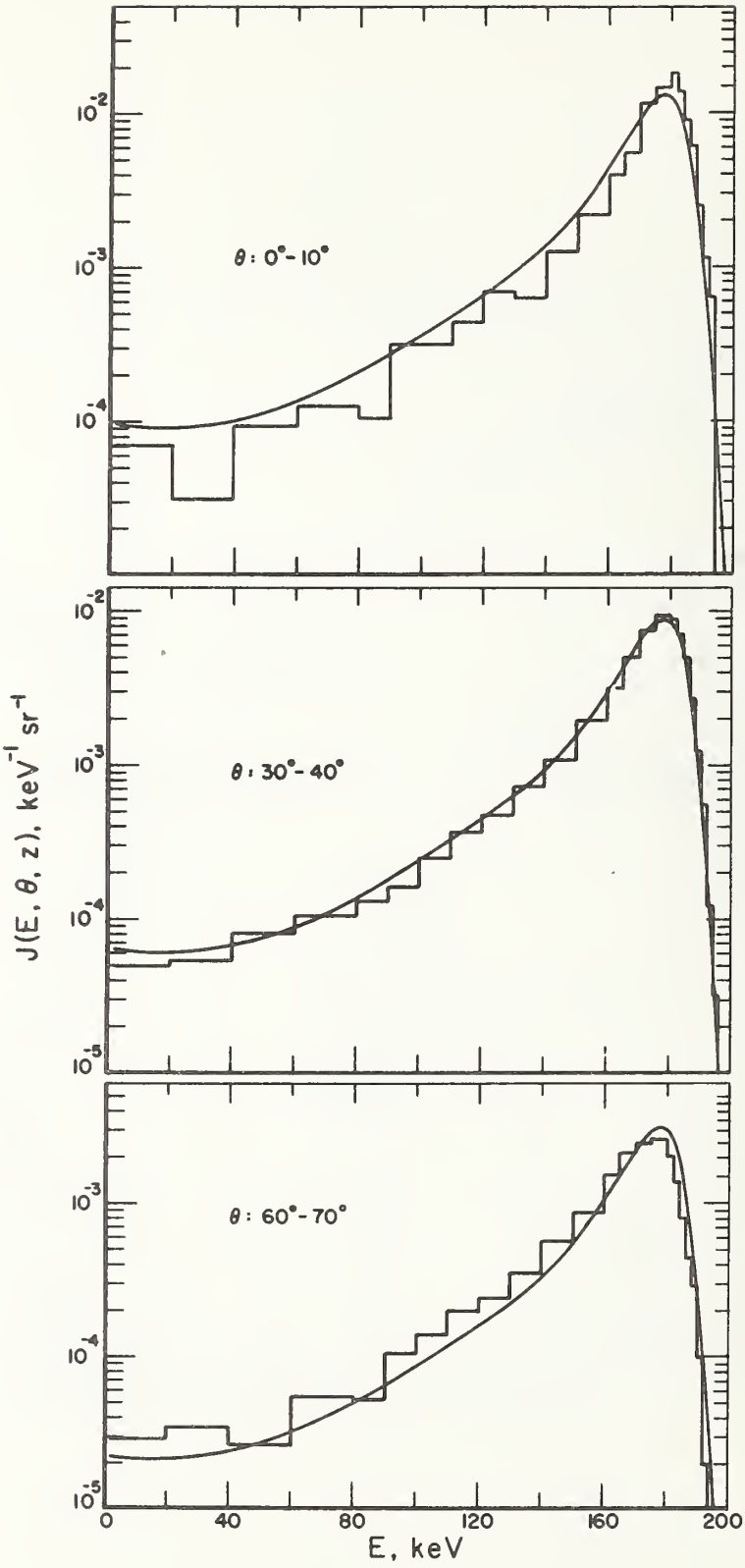

Figure 14

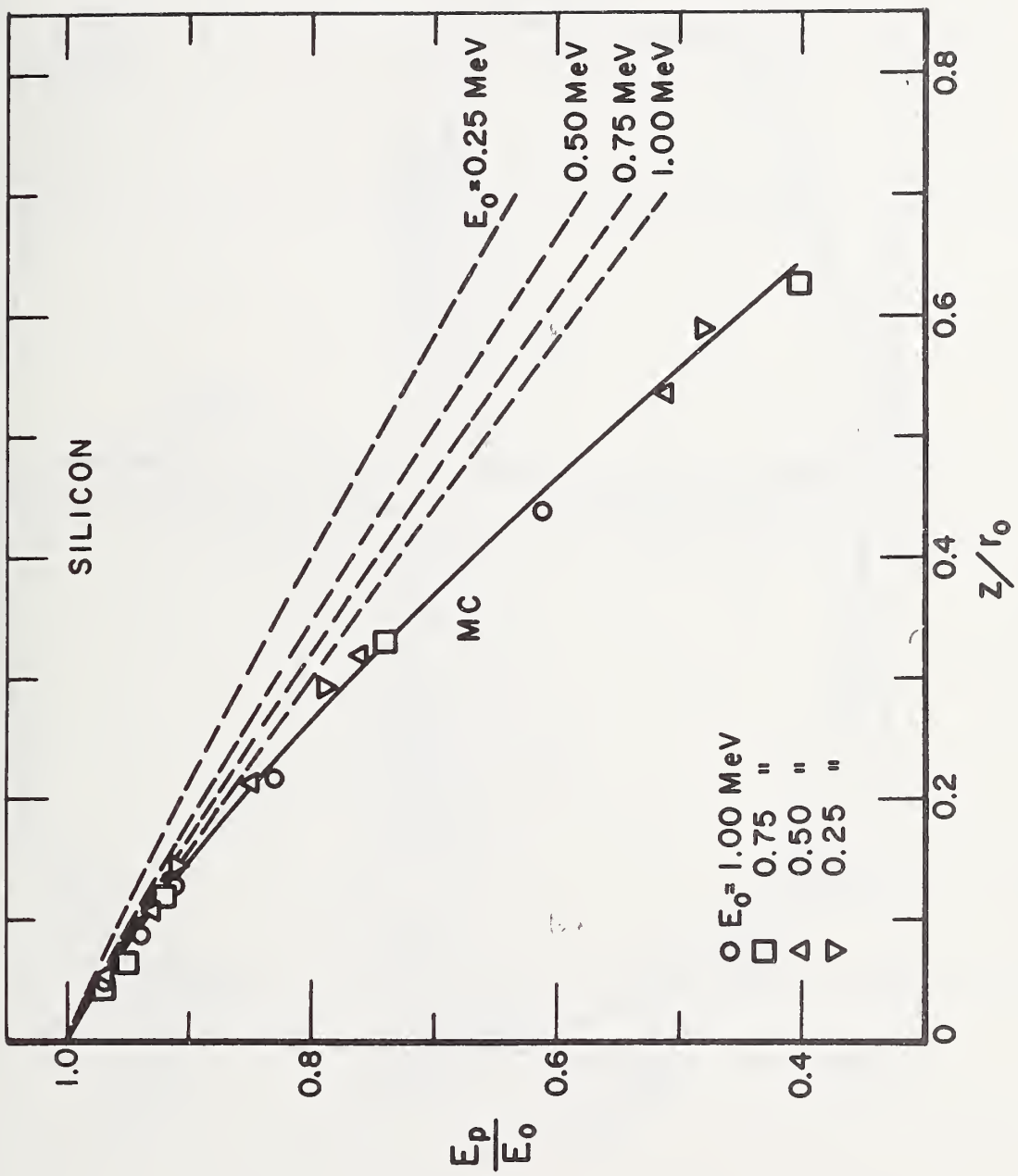
SILICON
E_o=0.25 MeV
0.50 MeV
0.75 MeV
1.00 MeV
MC
O E_o= 1.00 MeV
□ 0.75 "
△ 0.50 "
▽ 0.25 "
E_p/E_o
Z/r_o
1.0
0.8
0.6
0.4
0
0.2
0.4
0.6
0.8

Figure 15

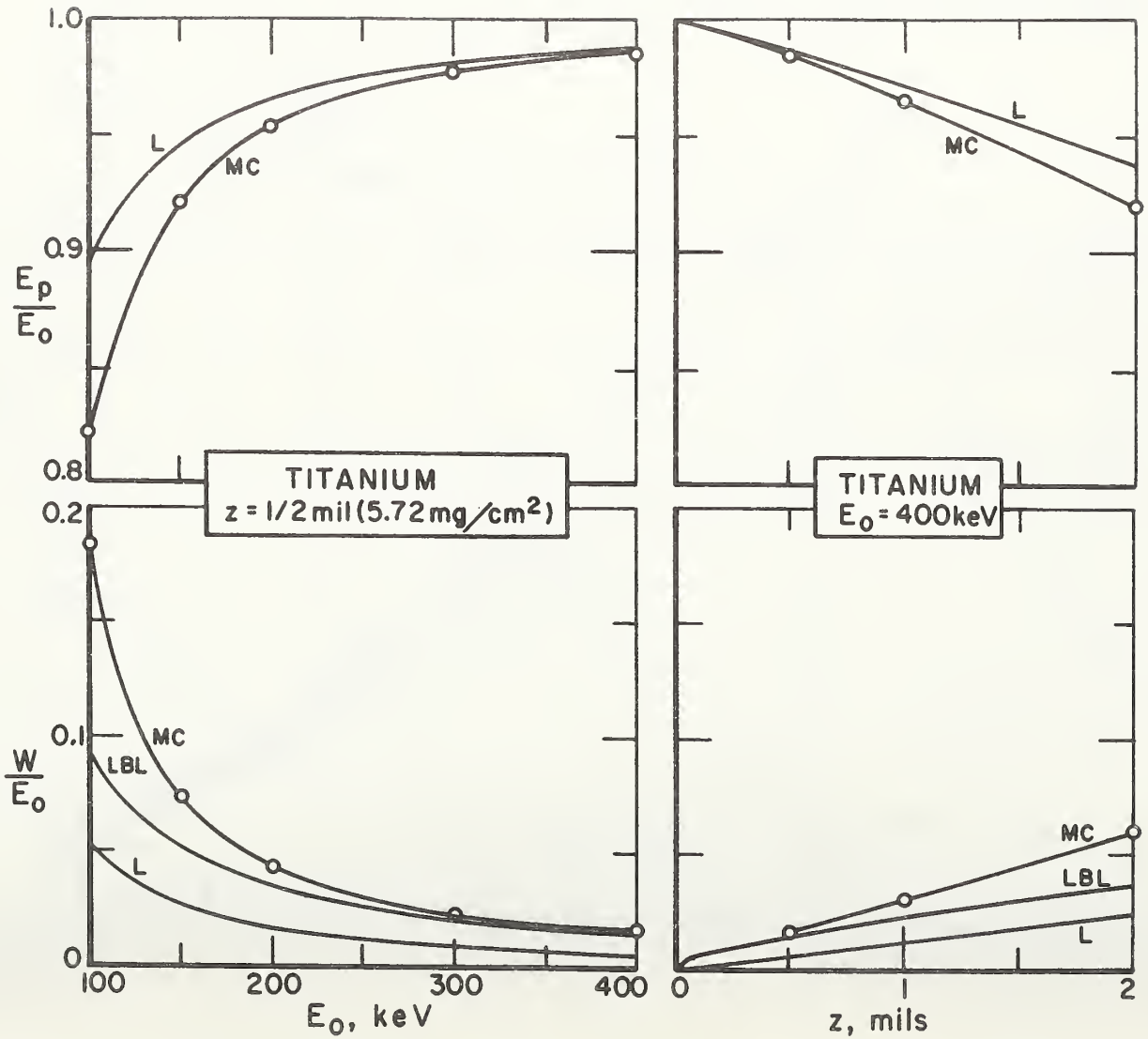
1.0
0.9
0.8
$\frac{E_p}{E_0}$
L
MC
TITANIUM
z = 1/2 mil (5.72 mg/cm²)
TITANIUM
E₀ = 400 keV
0.2
0.1
0
$\frac{W}{E_0}$
MC
LBL
L
100
200
300
400
E₀, keV
0
2
z, mils

Figure 16

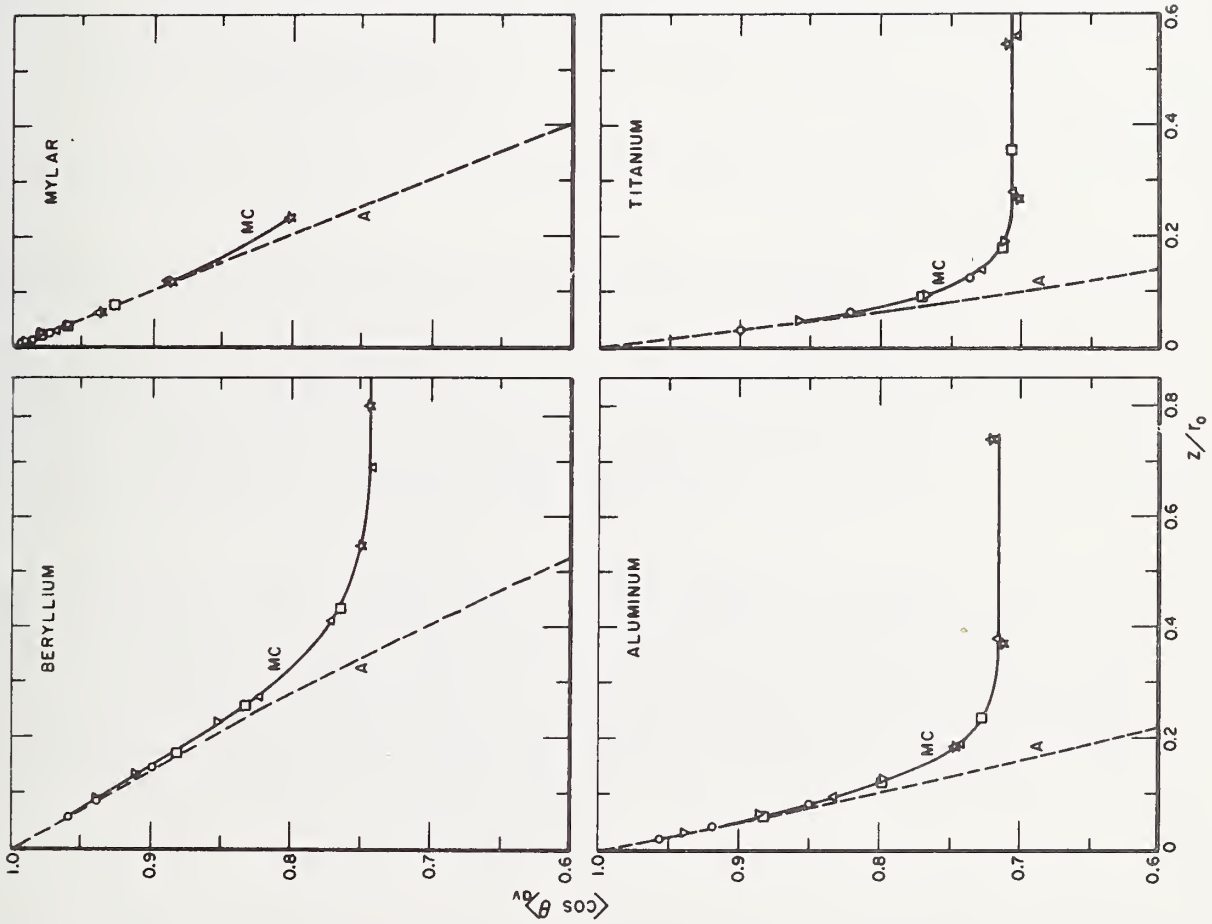
MYLAR
TITANIUM
BERYLLIUM
ALUMINUM
MC
A
1.0
0.9
0.8
0.7
0.6
0
0.2
0.4
0.6
0.8
$\langle \cos\theta \rangle_{dv}$
z/r_0

Figure 17

NBS 1143A (REV. 7-73)

U.S. DEPT. OF COMM. BIBLIOGRAPHIC DATA SHEET	1. PUBLICATION OR REPORT NO. NBSIR 74-457	2. Gov't Accession No.	3. Recipient's Accession No.

4. TITLE AND SUBTITLE: Transmission of Electrons Through Foils

5. Publication Date

6. Performing Organization Code

7. AUTHOR(S): Stephen M. Seltzer

8. Performing Organ. Report No. NBSIR 74-457

9. PERFORMING ORGANIZATION NAME AND ADDRESS

NATIONAL BUREAU OF STANDARDS
DEPARTMENT OF COMMERCE
WASHINGTON, D.C. 20234

10. Project/Task/Work Unit No. 2400439

11. Contract Grant No.

12. Sponsoring Organization Name and Complete Address (Street, City, State, ZIP)

Office of Naval Research
Arlington, Virginia 22217

13. Type of Report & Period Covered

14. Sponsoring Agency Code

15. SUPPLEMENTARY NOTES

16. ABSTRACT (A 200-word or less factual summary of most significant information. If document includes a significant bibliography or literature survey, mention it here.)

The transmission of electrons through foils has been studied by a Monte Carlo method. Cases involving electrons with energies from 50 keV to 1 MeV normally incident on beryllium, mylar, aluminum, and titanium foils are considered. Good agreement with experimental results has been found for quantities such as the number transmission, the energy and angular distribution of the emergent electrons, and the spatial distribution of energy deposited in the foil.

A comprehensive set of results has been generated for 100, 150, 200, 300 and 400-keV electrons incident on beryllium, mylar, aluminum, and titanium foils that are commonly used as vacuum windows in conjunction with low energy electron accelerators. Quantities given are the electron number and energy transmission and reflection, the energy absorbed, and the energy and angular distribution of the transmitted electrons. It is shown that much of the results can be presented in a scaled form which reduces the explicit dependence on, and facilitates the interpolation with respect to, the incident energy.

17. KEY WORDS (six to twelve entries; alphabetical order; capitalize only the first letter of the first key word unless a proper name; separated by semicolons) Angular distribution; electrons; energy spectra; reflection; transmission; transport calculation

18. AVAILABILITY

[X] Unlimited

[ ] For Official Distribution. Do Not Release to NTIS

[ ] Order From Sup. of Doc., U.S. Government Printing Office Washington, D.C. 20402, SD Cat. No. C13

[ ] Order From National Technical Information Service (NTIS) Springfield, Virginia 22151

19. SECURITY CLASS (THIS REPORT) U UNCLASSIFIED	21. NO. OF PAGES 83
20. SECURITY CLASS (THIS PAGE) UNCLASSIFIED	22. Price

USCOMM-DC 29042-P74

AMERICAN REVOLUTION BICENTENNIAL 1776-1976